International Journal of Fatigue, Volume 176, November 2023, Article number 107829
DOI:10.1016/j.ijfatigue.2023.107829

Crystal plasticity constitutive model and thermodynamics informed creep-fatigue life prediction model for Ni-based single crystal superalloy

Pin Lu[a], Xiaochao Jin[a], Pan Li[a], Yongle Sun[b], Xueling Fan[a*]

[a]*Xi'an Key Laboratory of Extreme Environmental Serviceability and Protection Technologies, School of Aerospace Engineering, Xi'an Jiaotong University, Xi'an, 710049, China*

[b]*Welding and Additive Manufacturing Centre, Cranfield University, Cranfield MK43 0AL, UK*

Abstract

Ni-based single crystal superalloys are the main constituent materials for aeroengine turbine blades. They are subjected to extensive in-service plastic deformation and creep-fatigue interaction, which can cause damage and failure and hence limit the turbine blade durability. In this study, a novel crystal plasticity-based constitutive model is proposed to predict the cyclic inelastic deformation of Ni-based single crystal superalloy under creep-fatigue loads, and the key aspects examined include cyclic strain hardening, ratcheting and stress relaxation behavior. The novelty of the model lies in the introduction of a dislocation density parameter in the kinematic hardening rule to describe the evolutionary characteristics of hysteresis loops. The constitutive model is implemented via the crystal plasticity finite element method and the predictions are in good agreement with experimental results. Furthermore, thermodynamic entropy generation is innovatively adopted as an indicator parameter for analysis of Ni-based single crystal creep-fatigue failure, and the corresponding creep and fatigue damage models are developed to evaluate the degree of damage. The half-life concept associated with the steady-state hysteresis loop is employed in the failure model to predict the creep-fatigue life without being limited by the computational efficiency of

Published by Elsevier. This is the Author Accepted Manuscript issued with: Creative Commons Attribution Non-Commercial No Derivatives License (CC:BY:NC:ND 4.0).
The final published version (version of record) is available online at DOI:10.1016/j.ijfatigue.2023.107829. Please refer to any applicable publisher terms of use.

the crystal plasticity finite element method. The proposed model can well capture the characteristics of Ni-based single crystal creep-fatigue life, and the prediction falls within a scatter band of factor 2.0 compared to experimental results. The proposed creep-fatigue life prediction model is underpinned by deformation and failure mechanisms, which would provide a basis for accurate analysis and robust assessment of Ni-based single crystal superalloy performance and life.

Keywords: Crystal plasticity; Creep-fatigue interaction; Kinematic hardening; Entropy generation; Life prediction

*Corresponding authors. E-mail address: fanxueling@mail.xjtu.edu.cn (X.L. Fan);

1. Introduction

Single crystal superalloys possess outstanding high-temperature mechanical properties due to the unique two-phase microstructure. Ni-based single crystal superalloy has been widely used in the hot-end components of aeroengines exposed to complex service environment, and the harshness of the operation conditions seriously affects the life of the components. It has been recognized that the traditional low-cycle fatigue (LCF) test cannot accurately represent the mechanical loads of aeroengine hot-end components in service [1, 2]. The dwell time under a certain working condition significantly affects the service life of hot-end part. Therefore, the creep-fatigue interaction damage mechanism and the associated life prediction of Ni-based single crystal superalloy has become a hot topic under intense research over the past few years. The relationship between the damage mode of single crystal and dwell time is shown in Fig. 1. Single crystal materials exhibit a typical ductile fracture mode under LCF loading, where cracks initiate from the surface of the crystal and propagate inward. This behavior differs from that of polycrystalline materials [3]. Under creep-fatigue interaction, single crystals exhibit creep voids, which increase in both quantity and size with prolonged dwell time [4]. Therefore, the analysis of the mechanical response of Ni-based single crystal superalloy to creep-fatigue interaction is needed to understand the material damage mechanism and ensure the safe operation of hot-end components.

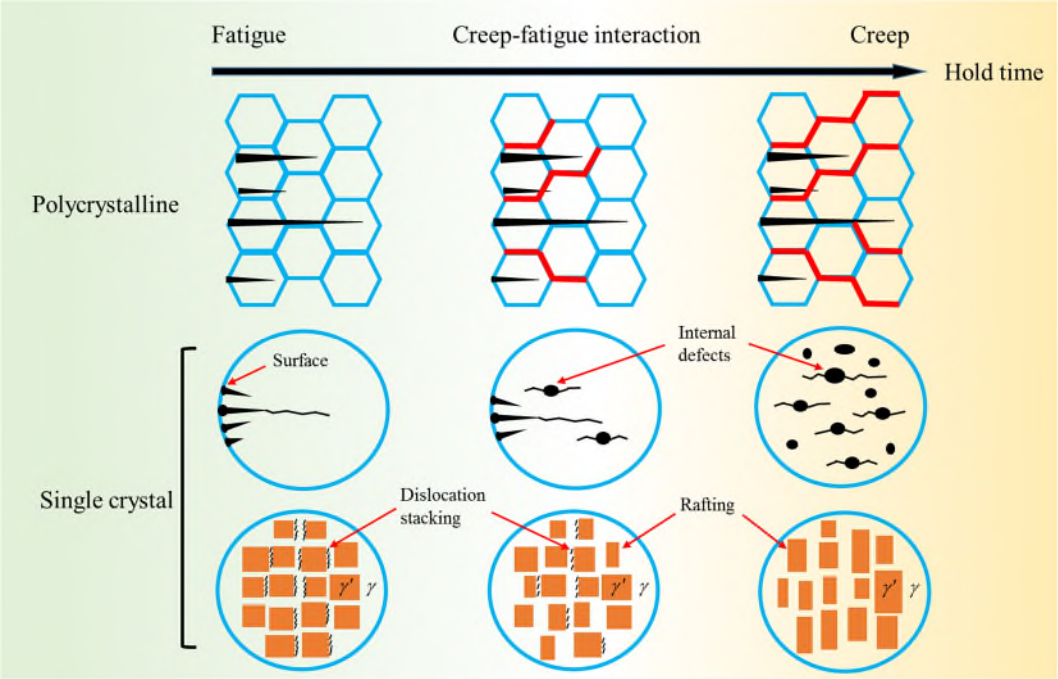

Fig. 1. Schematic diagram of the relationship between creep-fatigue damage mode and dwell time for polycrystalline and single crystal materials.

1.1 Literature review

Compared with pure fatigue, the damage mechanism of creep-fatigue interaction is more complex, which poses more difficulties in developing life prediction model. Early creep-fatigue life prediction models were primarily developed based on traditional fatigue life prediction models, including frequency-modified model [5], frequency separation model [6], frequency modified-damage function model [7], and their extended version [8, 9]. With the continuous exploration of the creep-fatigue coupling mechanism, life models based on linear damage summation (LDS) and nonlinear damage summation (NDS) rules have been proposed to accurately capture the creep-fatigue life distribution characteristics. In creep-fatigue life prediction based on LDS rule, the coupling of creep damage and fatigue damage is ignored. Typical applications such as time fraction model [10] and strain energy density exhaustion (SEDE) model [11]. Wang et al. [12] proposed a modified SEDE model by considering the effects of average stress and stress relaxation during the dwell time of creep-fatigue tests, and this model has also been successfully applied in multi-axial creep-fatigue conditions [13, 14]. In the NDS-based creep-fatigue life prediction model, creep damage and fatigue

damage are interdependent. Phenomenological theory is the most commonly used approach to accurately describe the degree of interaction between creep and fatigue [15, 16]. Although different strategies to improve the creep-fatigue life model have been proposed, most models established the relationship between life and physical parameters from the perspective of macroscopic phenomenology, which cannot reflect the influence of microstructural characteristics on creep-fatigue life and hence limits the predictive capability and robustness.

It is well known that ratcheting and stress relaxation are the main deformation characteristics under LCF and creep-fatigue loading [17, 18]. Previous research showed that adding a dynamic and static recovery term in the kinematic hardening model was effective to improve the prediction of ratchetting and stress relaxation deformation [19-22]. Some scholars have proposed complex combinations of multiple mechanisms and criteria to improve the predictive capability of the model [23]. However, due to the high computational cost, this calibration strategy has not been widely adopted. Therefore, it has become mainstream in research to develop kinematic hardening models with simpler forms to describe cyclic loading characteristics, mainly including Prager model [24], Armstrong-Frederick (A-F) model [25], Chaboche model [26], Ohno-Wang (O-W) model [27] and their extended versions [28, 29]. With a deeper understanding of the fundamental nature of material deformation, researchers have increasingly focused on incorporating the influence of microstructural mechanisms on flow stress into models. Li et al. [30] used the A-F model and two nonlinear kinematic hardening models to respectively describe the effects of dislocation slip, twinning and detwinning on the evolution of back stress in Mg alloy single crystal. The dislocation density was introduced as a controlling parameter for ratcheting deformation in the kinematic hardening model to enhance prediction capability [31]. The rafting parameters of the precipitate phase in Ni-based single crystal superalloys were introduced into the kinematic hardening model to predict ratcheting deformation [32]. For the stress relaxation response of materials, many meaningful attempts have been made, such as a two-step constitutive model combining creep and plasticity proposed by Daniel et al. [33], a kinematic hardening model considering static recovery [21], and the modified

Chaboche model with parameters corrected for dislocation network structure [34]. Although some models based on experimental observation of microstructure have great advantages in predicting macroscopic mechanical responses from microscale physical mechanisms, these are difficult to extend to other specific loading conditions due to the distinct microstructural characteristics.

The crystal plasticity finite element method (CPFEM) has been employed by many scholars to simulate the mechanical behavior of materials at the grain level. With the continuous development of computer power and finite element theory, the application of CPFEM has gradually expanded from the initial one-dimensional problem [35] to the present three-dimensional problem [36]. In phenomenological models, resolved shear stress serves as an intermediate variable in calculating the flow stress and is used to describe the behavior of the slip systems [36-39]. Dislocations, viewed as carriers of plastic deformation, are considered as internal variables in physics-based constitutive models. Continuously improved dislocation density evolution models as well as models that calculate the flow stress through dislocation density have been proposed by many scholars [20, 40-45]. With the continuous improvement of crystal plasticity theory, the CPFEM has become an important tool for studying creep-fatigue damage evolution and life prediction. Estrada Rodas et al. [20] proposed a crystal viscoplasticity model that considers several physics-based arguments to explain the deformation mechanism between material phases under creep-fatigue loading. Ding et al. [8] revealed the relationship between the microscopic deformation mechanism and macroscopic mechanical response under creep-fatigue loading in DZ445 alloy through experiments, and proposed a dislocation-based crystal plasticity model for creep-fatigue deformation. Li et al. [9] combined grain boundary cavity model and crystal plasticity model to analyze the creep-fatigue damage process and life of Inconel 718 superalloy from both macroscopic and microscopic scales. Based on the unique advantages of crystal plasticity finite element method in describing grain damage, various life prediction models related to slip system parameters have been developed, including cumulative plastic slip strain [46], cumulative energy dissipation [12], energy-based damage index [47], and their extended versions [48, 49].

Phenomenological models are based on empirical formulas to capture the macroscopic deformation characteristics of materials. As the mechanical characteristics of materials become increasingly complex, it becomes more and more difficult to describe their mechanical response through phenomenological models. Consequently, physics-based models have drawn widespread attention from scholars due to their clear physical meaning. However, compared with the widely used phenomenological model, the physics-based model is still not mature enough. Therefore, it is of great scientific significance to develop a physics-based crystal plasticity model for accurately capturing the mechanical response and life of Ni-based single crystals under different stress conditions.

1.2 Aim and scope

This study is aimed to develop constitutive model and life prediction model for Ni-based single crystal superalloy under creep-fatigue loading. A dislocation density-based single crystal constitutive model with modified kinematic hardening rule was developed to capture the ratcheting and stress relaxation behavior of Ni-based single crystals. Furthermore, thermodynamic entropy generation was considered as the indicator parameter for creep and fatigue damage, and a simplified calculation method was proposed in the crystal plasticity framework. The coupling of creep and fatigue damage was modelled through the LDS rule combined with NDS. The proposed single crystal life prediction model was validated using a series of strain-controlled uniaxial fatigue and creep-fatigue tests for DD6 superalloy at 760℃.

2. Crystal plasticity constitutive model

This section describes the formulation of the crystal plasticity constitutive model. The classical A-F kinematic hardening rule is modified in the framework of crystal plasticity theory, and the forest dislocation density is introduced into the dynamic and static recovery terms for accurately capturing the mechanical response of Ni-based single crystal to creep-fatigue loads.

In the crystal plasticity theory, the deformation of material can be represented by the deformation gradient tensor $\mathbf{F}$. It is generally assumed that the tensor $\mathbf{F}$ can be expressed as the product of elastic component $\mathbf{F_e}$ and plastic component $\mathbf{F_p}$.

$$\mathbf{F} = \mathbf{F}_e\mathbf{F}_p \tag{1}$$

where the reference configuration was transformed into an intermediate configuration through plastic deformation $\mathbf{F_p}$. Then the intermediate configuration was transformed into the current configuration through elastic deformation and rigid body rotation $\mathbf{F_e}$.

The plastic deformation and dislocation slip in slip systems can be interrelated through the crystal plasticity theory. Therefore, the velocity gradient $\mathbf{L_p}$ on the intermediate configuration can be represented as the sum of the shear strain rates $\dot{\gamma}$ of all slip systems.

$$\mathbf{L}_p = \dot{\mathbf{F}}_P\mathbf{F}_P^{-1} = \sum_\alpha \dot{\gamma}\mathbf{s}^\alpha\mathbf{m}^\alpha \tag{2}$$

where $\mathbf{s}^\alpha$ and $\mathbf{m}^\alpha$ are the slip direction of the slip system and the normal direction of the slip plane in the reference configuration, respectively.

In the rate-dependent crystal plasticity framework, the shear strain rate in the power-law form [50] is widely used, viz.

$$\dot{\gamma} = \dot{\gamma}_0\left|\frac{\tau^\alpha - \chi^\alpha}{g^\alpha}\right|^{\frac{1}{m}}\operatorname{sgn}(\tau^\alpha) \tag{3}$$

where $\dot{\gamma}^\alpha$, τ^α, g^α and χ^α are shear strain rate, shear stress, current strength and back stress of slip system α, respectively, m is the rate sensitivity exponent.

The current strength g^α of slip system α can be decomposed into linear accumulation of initial strength $g_0^\alpha(T)$ and subsequent strengthening $g_{for}^\alpha(T)$ as follows

$$g^\alpha = g_0^\alpha(T) + g_{for}^\alpha(T) \tag{4}$$

The initial strength parameter $g_0^\alpha(T)$ controlling the yield strength consists of the following three parts.

$$g_0^\alpha(T) = g_{0,ss}^\alpha(T) + g_{0,shear}^\alpha(T) + g_{0,loop}^\alpha(T) \tag{5}$$

where $g_{0,ss}^\alpha(T)$ is solid solution strengthening, $g_{0,shear}^\alpha(T)$ and $g_{0,loop}^\alpha(T)$ represent the effects of dislocation shearing precipitates and dislocation by-passing precipitates on the initial strength, respectively.

The solid solution strengthening term is derived based on the assumption that solutes

are distributed in the metal matrix without interacting with each other [51], which is given by

$$g_{0,ss}^{\alpha}(T)=\frac{1}{M}\sum\frac{d\sigma}{d\sqrt{g_i}}\sqrt{g_i} \tag{6}$$

where M is Taylor factor, $d\sigma/d\sqrt{g_i}$ is strengthening coefficient which indicates the strengthening capacity of each alloying element, $d\sigma/d\sqrt{g_i}$ and g_i are the strengthening coefficient and atomic fraction, respectively, which can be obtained from the authors' previous work [52], see Appendix B.

The study revealed that Ni-based single crystals exhibit anomalous yield characteristics at high temperatures, primarily attributed to the variations in precipitate strength with temperature [52]. The thermally activated cross-slip mechanism is considered the primary factor influencing the strength of precipitate phases in Ni-based single crystals. Therefore, in previous work by the author [52], the contribution of dislocation shearing precipitation to the strength was represented as a superposition of anti-phase boundary (APB) energy and thermally activated cross-slip mechanisms, as shown below.

$$g_{0,shear}^{\alpha}(T)=0.7G_{\gamma'}\left(\frac{APB_{\gamma'}^{\alpha}}{G_{\gamma'}^{\alpha}b_{\gamma'}^{\alpha}}\right)^{\frac{3}{2}}\left(\frac{af_{shear}r}{b_{\gamma'}^{\alpha}}\right)^{\frac{1}{2}}+f\left[B\exp\left[-\frac{(T-T_r)^2}{\xi}\right]+\frac{1}{M}\sum_i\left(\frac{d\sigma}{dC_i}C_i\right)\right] \tag{7}$$

where $G_{\gamma'}$ is shear modulus of γ' precipitates, b is Burgers Vector, $APB_{\gamma'}$ is antiphase boundary energy (see Appendix A), f_{shear} is volume fraction of dislocation shearing precipitation mechanism, r is average size of γ' precipitates, T and T_r are current temperature and reference temperature corresponding to the maximum slip strength, respectively, ξ, B and $d\sigma/dC_i$ are material constants and the values are taken from Ref. [52] (see Appendix B).

As dislocation by-passing precipitation accompanies dislocation shearing precipitation in the concerned temperature range, the strengthening effect produced by dislocation by-passing precipitates is also considered in our model. Here, we adopt the theory originally developed by Orowan et al. [53] and later extended by Ashby et al. [54], and the contribution of dislocation by-passing precipitation to the strength is

expressed as follows

$$g_{0,loop}^{\alpha}(T)=\frac{1}{M}\frac{0.3Gb\sqrt{f_{loop}}}{r}\ln(\frac{r}{2b}) \tag{8}$$

where f_{loop} is volume fraction of dislocation by-passing precipitates mechanism.

The isotropic work hardening can be interpreted as the effect of dislocations stored in the crystals on the continued slip. Here, the forest dislocation density-based strengthening model modified by M.G. Lee et al. [55] is adopted to describe the work hardening, viz.

$$g_{for}^{\alpha}(T)=b^{\alpha}G^{\alpha}(T)\sqrt{h^{\alpha\alpha'}\rho_{for}^{\alpha'}} \tag{9}$$

where matrix $h^{\alpha\alpha'}=n^{\alpha}\cdot t^{\alpha'}$ can be obtained through the geometry of edge dislocations on each slip system. A detailed description can be found in reference [56]. The $\rho_{for}^{\alpha'}$ is the forest dislocation density on different slip systems. It has been proved that the phenomenological storage-recovery model proposed by Kocks [57] is suitable for describing the evolution of macroscopic dislocation density. Therefore, the evolution function of dislocation density at different temperatures can be expressed as

$$\frac{\partial\rho_{for}^{\alpha}}{\partial\gamma^{\alpha}}=k_1^{\alpha}\sqrt{\rho_{for}^{\alpha}}-k_2^{\alpha}(\dot{\varepsilon},T)\rho_{for}^{\alpha} \tag{10}$$

where k_1 and k_2 represent the adjustable coefficient of dislocation generation and annihilation, respectively. Essmann and Mughrabi [58] found that the dislocation annihilation parameter (k_2) is dependent on temperature and strain rate, while dislocation generation is rate insensitive (below 10^3 s^{-1}). Therefore, it is reasonable to treat the dislocation generation parameter (k_1) as a material constant, while the dislocation annihilation parameter (k_2) is dependent on the specific thermal and mechanical loads. Here, the evolution model of dislocation annihilation is based on the thermal activation theory of plastic deformation [59], viz.

$$\frac{k_2^{\alpha}}{k_1^{\alpha}}=\frac{\bar{\chi}b^{\alpha}}{Q_1^{\alpha}}(1-\frac{kT}{D^{\alpha}b^3}\ln(\frac{\dot{\varepsilon}}{\dot{\varepsilon}_0})) \tag{11}$$

where $\bar{\chi}$ is the interaction parameter, which is set to be 0.9 [60]. The parameters D, Q, k and $\dot{\varepsilon}$ are drag stress, effective activation enthalpy, Boltzmann constant and

strain rate, respectively. The reference strain rate $\dot{\varepsilon}_0$ is taken to be 10^7 s^{-1} [60].

The kinematic hardening arises from Bauschinger effect during cyclic deformation and it can be modelled using the back stress. The classical A-F kinematic hardening model is represented as follows.

$$\dot{\chi}^{\alpha} = C_1 \dot{\gamma}^{\alpha} - C_2 \chi^{\alpha} \left| \dot{\gamma}^{\alpha} \right| \tag{12}$$

where C_1 is hardening coefficient and C_2 is dynamic recovery coefficient, respectively, which are material constants and set to be the same value in different slip systems. The classic A-F kinematic hardening rule had greatly promoted the development of related plasticity theory. However, as new alloys exhibit more complex deformation mechanisms, modification of the classic A-F model for improving prediction accuracy is needed, which will be described in the next section.

3. Improved kinematic hardening rule

The study of kinematic hardening models can be traced back to Prager's work [61], where a model was proposed that exhibits a linear relationship between the evolution of back stress and plastic strain. However, the Prager model would lead to cyclic elastic or plastic shakedown, which could not capture the ratcheting phenomenon. Therefore, Armstrong and Frederick [62] modified Prager linear dynamic hardening model and introduced dynamic recovery term. Furthermore, Chaboche [63] proposed a kinematic hardening model with better simulation results by introducing significantly different recovery constants based on A-F model. So far, the theoretical basis of almost all back stress evolution models is derived from the abovementioned models.

3.1 Modification of dynamic recovery term of kinematic hardening rule

Macroscopic models are usually established based on objective laws, which lack clear physical meaning. Therefore, constitutive model considering microscopic physical mechanism has become an important trend. It is well known that dislocation slip is the carrier of crystal deformation. It is thus unsurprising that the micro parameters used to express the degree of dislocation slip have become the research focus of many scholars. It has been found that the dislocation configuration gradually evolves from low-density dislocation lines, light dislocation entanglement and pile-ups to high-

density dislocation entanglement, walls and veins during uniaxial ratcheting deformation [64]. Shenoy et al. [65] adjusted the ratio of back stress to shear stress of each slip system by introducing phenomenological parameter into the linear hardening term. Based on the above research, it can be concluded that ratcheting deformation is related to dislocation movement. Therefore, it is appropriate to modify the kinematic hardening rule by considering dislocation density. Based on the work of Shenoy et al. [65], a modified nonlinear dynamic recovery term is established here by introducing forest dislocation density and volume fraction of precipitated phase, viz.

$$C_2 = \frac{\eta_0 f \dfrac{Z_1}{\boldsymbol{b}\lambda^{\alpha}}}{\dfrac{Z_1}{\boldsymbol{b}\lambda^{\alpha}} + Z_2\sqrt{\sum_{\alpha=1,12}\rho_{for}^{\alpha}}} \tag{13}$$

where, $\boldsymbol{b}$, λ , f and ρ_{for}^{α} are Burgers vector, spacing of precipitates, volume fraction of precipitates and forest dislocation density, respectively. The parameters η_0, Z_1 and Z_2 are material constants. Only the octahedral slip system needs to be considered in the [001] orientation [32]. In addition, the total dislocation density of all slip systems is used to simplify the model. It should be noted that the newly proposed dynamic recovery parameter C_2 has a similar form to the model proposed by Shenoy et al. [65]. The difference is that in our model the nonlinear parameter controlled by dislocation density and volume fraction of precipitates are linked with dynamic recovery term, which is beneficial to improve the convergence of CPFEM and capture ratcheting deformation.

3.2 Modification of static recovery term of kinematic hardening rule

It is widely recognized that adding static recovery term to kinematic hardening rule is necessary to simulate time-dependent deformation in cyclic loading. On the one hand, the traditional kinematic hardening rule with constant static recovery term cannot reproduce the cyclic stress relaxation behavior [66]. On the other hand, the dislocations-dislocations interaction and dislocations-precipitates interactions are the main deformation mechanisms during stress relaxation, which is the incentive and theoretical basis for modifying the kinematic hardening rule [67]. It should be noted that although Chaboche framework with multiple back stress components has better prediction

accuracy than the classical A-F model with single back stress component in the crystal plasticity theory, the more unknown parameters introduced by the Chaboche model may not be conducive to the practical applications and further development. Therefore, a modified nonlinear kinematic hardening rule is proposed here based on the classic A-F model, which introduces a new decreased static recovery term expressed as follows

$$\dot{\chi}^{\alpha} = C_1\dot{\gamma}^{\alpha} - C_2\chi^{\alpha}\left|\dot{\gamma}^{\alpha}\right| + C_3\chi^{\alpha} \tag{14}$$

$$C_3 = r_0[\varphi_s + (1-\varphi_s)e^{C_4}] \tag{15}$$

$$C_4 = -\frac{\sum_{\alpha=1}^{12}\rho_{for}^{\alpha}}{\rho_r} \tag{16}$$

where the established static recovery coefficient C_3 is set as an exponential function related to total forest dislocation density, r_0 and φ_s are material constants representing the degree of static recovery, ρ_r is the reference dislocation density, which controls the decaying rate of stress relaxation with the number of load cycles. It is worth noting that the introduced attenuation function C_3 is similar to the static recovery term in Xuan's model [21]. However, unlike Xuan's model the total forest dislocation density, the intuitive embodiment of dislocation movement and the number of dislocations, are used to replace the accumulated inelastic strain. Apparently, the static recovery term is controlled by φ_s. If $\varphi_s = 1$, the model reduces to the classical A-F model. If $\varphi_s < 1$, parameter C_3 decreases with the increase of dislocation density. If $\varphi_s > 1$, the increased dislocation density leads to a larger value of C_3.

4. Fatigue and creep damage model

Most empirical life prediction models are defined as the direct correlations between some selected parameters (for instance, strain range, stress amplitude, etc.) and the number of load cycles. Typical examples of these models include Manson-Coffin model [5] and frequency modified life model [6]. Although empirical models for life prediction have good accuracy for certain materials after calibration, its predictive capability is usually limited and does not shed light on the microscopic mechanisms responsible for the material failure. With the development of continuum damage

mechanics (CDM), life prediction model also adopts the damage theory. The concept of damage was originally proposed by Kachanov [68] to describe the process that the macroscopic performance of materials gradually degrades until the failure occurs. Damage parameter is an internal state variable used to describe the damage state and its evolution. Typically, the cyclic number is considered as the life of material when damage reaches critical value. Therefore, accurately characterizing the material's damage state is crucial for establishing a damage-based life prediction model.

The second law of thermodynamics indicates the irreversibility of thermodynamic processes, known as the entropy increase law. Therefore, thermodynamic entropy naturally serves as a fundamental metric to quantify various behaviors in irreversible processes. Despite the dependence of damage mechanisms on materials, it is reasonable to consider the degradation process of material performance as a sum of irreversible processes that contribute to an increase in system disorder. Consequently, the damage state can be described by the thermodynamic entropy. Ital [69] conducted early research on the theory of thermodynamics entropy generation. They put forward the entropy criteria for the failure of deformed solid, and derived the integral and differential forms of entropy generation function. The cumulative entropy of different materials at fracture point was defined as the fracture fatigue entropy (FFE), which is solely determined by the material and independent of geometry and load amplitude and frequency [70]. In addition, it proved that the normalized entropy was approximately proportional to the normalized number of load cycles. Amiri and Modarres [71] discussed in detail the progress of entropy generation in describing damage, and proposed a thermodynamic framework using entropy generation as a measure of material damage. Furthermore, the fatigue life of low-carbon steel was predicted using entropy generation [72]. Compared with the traditional empirical models, the damage model based on thermodynamic entropy has more clear physical meaning, which is helpful to understand the nature of material failure.

Based on the Clausius-Duhem inequality, the entropy generation rate can be expressed as follows.

$$\dot{S} = \frac{W_p}{T} - \frac{1}{T} A_k \dot{V}_k - \frac{1}{T^2} \mathbf{q} \cdot \mathbf{grad} T \tag{17}$$

where $\dot{S}$ is entropy generation rate, T is temperature, $W_p = \sigma : \dot{\varepsilon}^p$ is plastic work, $\dot{V}_k$ and A_k represent the internal variable changing rate and the thermodynamic force related to the internal variable, respectively, and $\mathbf{q}$ is defined as the thermal flux. The entropy generation rate consists of three parts: entropy generation caused by plastic dissipation ($W_p = \sigma : \dot{\varepsilon}^p$), entropy generation caused by internal variables ($A_k \dot{V}_k$) and entropy generation due to heat conduction ($1/T^2 \cdot \mathbf{q} \cdot \mathbf{grad} T$). It should be mentioned that $A_k \dot{V}_k$ is the non-recoverable energy stored in the material, which is often negligible for metallic materials ($A_k \dot{V}_k \approx 0$) [70]. Therefore, Eq. 17 can be simplified as follows

$$\dot{S} = \frac{W_p}{T} - \frac{1}{T^2} \mathbf{q} \cdot \mathbf{grad} T \tag{18}$$

As mentioned earlier, dislocation slip is the main form of crystal deformation. In the crystal plasticity framework, the entropy generation within each load cycle is calculated via the shear stress and shear strain rate on all slip systems, as shown below [16].

$$\Delta S = \int_{cycle} \left[\sum_{\alpha=1}^{12} (\tau^\alpha - \chi^\alpha) \dot{\gamma}^\alpha \right] \frac{\Delta t}{T(t)} - \frac{1}{T(t)^2} \mathbf{q} \cdot \mathbf{grad} T \Delta t \tag{19}$$

It should be noted that thermodynamic entropy generation can be seen as a measure of the irreversibility of a process in a system. Therefore, the temperature gradient in Eq. 19 should be attributed to the irreversible processes in the system rather than environmental constraints. Since previous studies found that the temperature change on the material surface was small during the low-cycle fatigue process at room temperature [73], the entropy generation due to heat conduction is usually negligible at room temperature. The temperature induced by irreversible processes under high-temperature fatigue loading in the specimen is considered to be approximately constant, which means that the temperature gradient can be ignored, viz. $\mathbf{grad} T \approx 0$. Based on the above discussion, it is assumed that the entropy generation caused by heat conduction can be also ignored for fatigue under constant high temperature. Consequently, our

model only considers the entropy generation caused by plastic deformation and the Eq. 19 is further simplified as follows.

$$\Delta S = \int_{cycle} \left[\sum_{\alpha=1}^{12} (\tau^{\alpha} - \chi^{\alpha}) \dot{\gamma}^{\alpha} \right] \frac{\Delta t}{T(t)} \tag{20}$$

Based on the general form of static toughness degradation after fatigue (Eq. 21) [74], Naderi and Khonsari [70] developed a thermodynamic entropy-based fatigue damage variable through combining the linear relationship between normalized entropy generation and normalized number of load cycles, as shown in Eq. 22.

$$D_f = A + B \ln(1 - N/N_f) \tag{21}$$

$$D_f = D_0 + \frac{(D_{f,c} - D_0)}{\ln(1 - S_c / S_g)} \ln(1 - S / S_g) \tag{22}$$

where D_f, D_0, $D_{f,c}$ are dimensionless fatigue damage parameter, initial damage and critical damage, respectively, S, S_g, S_c are current entropy generation, total entropy generation at fracture and critical entropy generation, respectively, and A and B are material constants.

The introduction of a creep damage model is the key point in building a creep-fatigue damage model, and it is of great significance for improving the prediction accuracy of the model. Compared to traditional elastoplastic models, thermodynamic models are consistent with physics as a mechanical model starting from the basic laws of thermodynamics. From the perspective of damage accumulation, thermodynamic entropy is closer to the nature of material damage than traditional elastoplastic parameters, such as energy dissipation. Therefore, based on the work of Payten et al. [75], the thermodynamic entropy generation is tentatively used to replace traditional parameters related to elastoplastic theory for the calculation of creep damage in the dwell stage, and the revised formulation is shown below.

$$D_c = \int_0^{t_d} \frac{1}{\varphi} [\dot{S}_{in}]^{1-n_1} dt \tag{23}$$

$$\varphi = B_1 \exp(\frac{-Q}{RT}) \tag{24}$$

where $\dot{S}_{in}$ is the entropy generation rate in the dwell stage, which is calculated by Eq. 20.

5. Constitutive model validation

The constitutive model established in this work was implemented via the user-defined material subroutine (UMAT) of ABAQUS/Standard software to simulate the creep-fatigue deformation of single crystal material. The UMAT was originally developed by Huang [76], which has been modified here to verify the predictive ability of the proposed single crystal plasticity constitutive model. The strain range considered in this study was small (<5%), that is, the deformation of the specimen was expected to be uniform. Therefore, a single-element model was adopted to enhance computational efficiency, and such a strategy was also accepted by other scholars [77]. The full integration hexahedral element (ABAQUS designation: C3D8) was used. For the two faces perpendicular to the loading axis, one was assigned with specified different displacements to impose various loads, and the other was fixed with respect to the axial displacement. The remaining four faces in the model were parallel to each other in pairs, and two adjacent faces were set as free boundaries while the other two conformed to symmetry boundary conditions. The schematic diagram of the boundary conditions and loading waveforms are shown in Figs. 2 and 3, respectively.

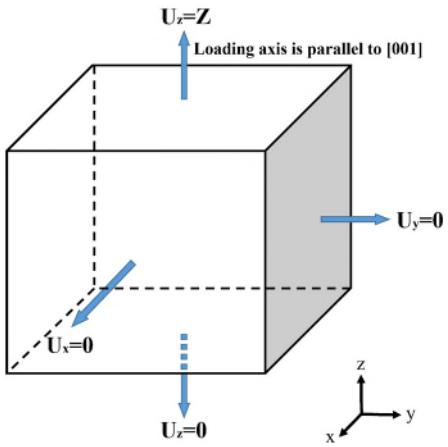

Fig. 2. The schematic diagram of the boundary conditions.

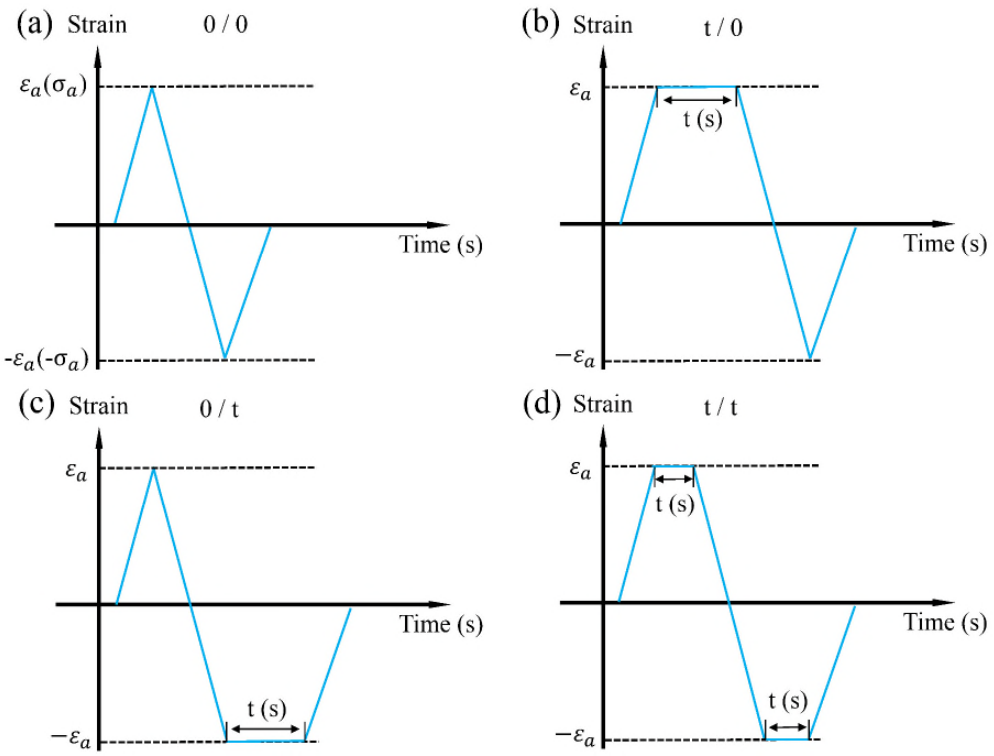

Fig. 3. The strain-controlled and stress-controlled loading waveforms used in the simulations: (a) without dwell-period (0/0), (b) with tension peak strain dwell-period (t/0), (c) with compression peak strain dwell-period (0/t) and (d) with tension/compression peak strain dwell-period (t/t).

The experimental data [78, 79] for uniaxial tension and creep-fatigue tests of Ni-based single crystal DD6 with [001] orientation at 760 ℃ were used to determine the material parameters in the constitutive model. It should be noted that the focus of this study is on the uniaxial creep-fatigue interaction with constant temperature and hence the experimental data at a typical high temperature of 760 ℃ were adopted. The calibration process of the single crystal constitutive model parameters include the following steps:

(1) The elastic constants (C_{11}, C_{12}, C_{44}) can be obtained via uniaxial tension tests and the data were from open literature [32]. The Burgers vector and shear modulus were taken from Refs. [80] and [81], respectively. The Boltzmann constant k and universal gas constant R are 1.38×10^{-20} mJ/K and 8.314 J/(mol·K), respectively. The APB energy of DD6 single crystal was taken as 200 mJ/m^2 [52]. The average size r, volume fraction f, and spacing λ of the precipitates can be obtained from the microstructure of the

DD6 superalloy [82]. The physical properties, such as linear expansion coefficient $\bar{\alpha}$, isochoric specific heat C_v, molar enthalpy of vaporization ΔH_B and molar enthalpy of fusion ΔH_M, among others, were taken from the material handbook [83]. The parameters (ρ_0, k_1, $\bar{\chi}$, Q_1, D, ξ and $\dot{\varepsilon}_0$) that control the evolution of the dislocation density cannot be obtained directly from experiments. Therefore, it is necessary to use the trial-and-error method to obtain these parameters through fitting the tension test data [52].

(2) The parameters used in the modified A-F kinematic hardening model need to be extracted from the cyclic loading curve through trial-and-error fitting. The parameters η_0, Z_1, Z_2 for modifying the dynamic recovery term and the parameters r_0, φ_s, ρ_r for modifying the static recovery term were determined using previous cyclic hardening [79] and stress relaxation [84] test data.

(3) In the calculation of fatigue damage, the parameter D_0 was usually set to be 0, indicating that there was no preexistent damage. Here we defined the critical damage parameter $D_{f,c}$ equal to 0.9, which is a reasonable value considering the measurement uncertainty of the experiment and the convergence of the finite element simulation [70]. Accordingly, the following formula holds as an approximation, i.e. $S_c = 0.9 S_g$, in which the total entropy generation parameter S_g cannot be directly measured in experiment and hence it was inferred through fitting the strain-controlled fatigue and creep-fatigue life data. The other two parameters B_1 and n_1 were also determined in a similar way.

It should be noted that for model verification purpose the microstructural parameters, such as the volume fraction, shape and spacing of the precipitated phase, were set to the values corresponding to the initial microstructure at the given constant temperature. The dependence of these parameters on the temperature and time should be considered when the model is used to assess prolonged creep-fatigue interaction at different high temperatures. All the physical parameters and optimal fitting parameters used in the model are summarized in Tables 1-3.

Table 1. The chemical components (wt.%) of Ni-based single crystal DD6 superalloy

[80].

Elements	Co	Cr	Mo	W	Re	Ta	Hf	Al	Ni
wt.%	9	4.3	2	8	2	7.5	0.1	5.7	Bal.

Table 2. Physical parameters of Ni-based single crystal DD6 superalloy.

Symbols	Value	Symbols	Value
b	0.253 nm	$\bar{\alpha}(T)$	13.53×10^{-6}
G	115 GPa	C_v(T)	0.6 J/(g·K)
r	450 nm	ΔH_M	17472 J/mol
k	1.38×10^{-20} mJ/K	ΔH_B	369251 J/mol
$APB_{\gamma'}(T_0)$	200 mJ/m^2	λ	100 nm
f	70 %	R	8.314 J/(mol·K)

Table 3. Material parameters obtained by fitting test data.

Symbols	Value	Symbols	Value
C_{11}	194 GPa	C_{12}	117.4 GPa
C_{44}	105 GPa	C_1	1×10^6
$\dot{\gamma}_0$	0.03	ρ_0	2×10^8 mm^{-2}
n	0.02	k_1	25
T_r	1123 K	χ	0.9
Q_1	0.3	a	0.02
D	$D=5E4+5E6\exp(-\frac{(T-1033)^2}{1500})$	ξ	25000
$\dot{\varepsilon}_0$	10^7	B	B=135-1.5(T-T$_r$)
M	3.06	η_0	5×10^4
Z_1	1.0	Z_2	1×10^3
r_0	-0.36	φ_s	10.0
ρ_r	2×10^9	D_0	0

D_c	0.9	S_g	0.38 mJ/(mm^{3}K)
S_c	0.9 S_g	B_1	$B_1 = 389501 - 630849 \times \varepsilon_a + 257797 \times \varepsilon_a^2$
Q	6.97×10^{-19} J/atom	n_1	0.6

The stress amplitude evolution curve with a strain amplitude of 1.0 % and the creep-fatigue cyclic stress-strain curves with tension peak strain dwell-period of 60 s (60/0) were regarded as references for calibration of the crystal plasticity model. The comparisons of experimental and modelling results for stress amplitude evolution curve and hysteresis loops of strain-controlled fatigue with different strain amplitudes are shown in Figs. 4 and 5. The proportion of inelastic strain in the hysteretic loop gradually rises with increasing strain amplitude, which is the main reason for the difference in alloy life. In addition, the creep-fatigue hysteresis curve predicted by the model, along with the experimental reference test curve, are shown in Fig. 6. A simple error calculation formula $|Exp. - Sim.|/Exp. \times 100\%$ is accepted to quantify the accuracy of the model. It can be found from Figs. 4-6 that the maximum error of stress amplitude is 2.3% for the cyclic loading with the strain amplitude of 1.2%. The maximum error of predicting creep-fatigue mechanical behavior with compression peak strain dwell-period of 60 s (0/60) and tension/compression peak strain dwell-period of 30 s (30/30) are 6.9% and 6.1%, respectively. The experimental results are in good agreement with the simulation ones, which proves that the developed crystal plasticity constitutive model can accurately capture the mechanical response of Ni-based single crystal DD6 under different loading conditions, including strain-controlled fatigue and creep-fatigue.

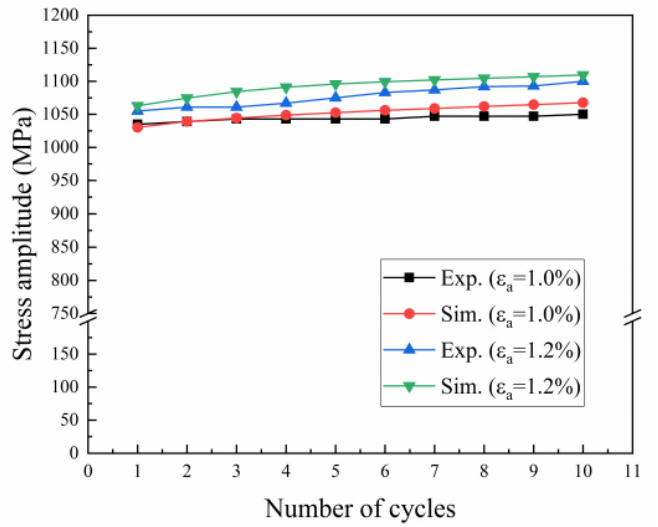

Fig. 4. Evolution of stress amplitude with the number of pure fatigue load cycles for experiments and simulations under strain amplitudes of 1.0% and 1.2%.

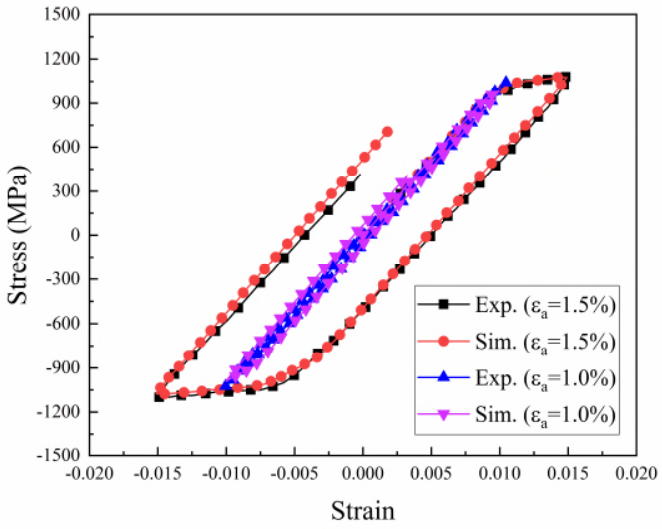

Fig. 5. Experimental and simulated pure fatigue cyclic stress-strain curves at strain amplitudes of 1.0% and 1.5%.

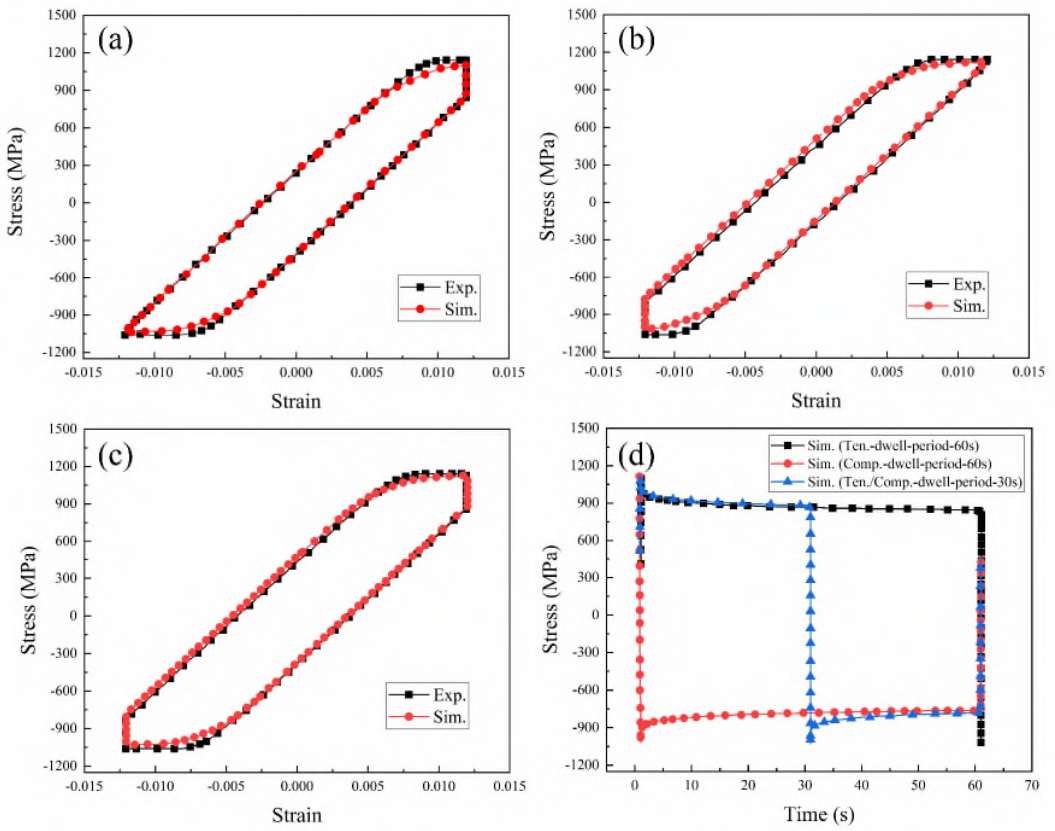

Fig. 6. Experimental and simulated creep-fatigue cyclic stress-strain curves: (a) with tension peak strain dwell-period of 60 s (60/0), (b) with compression peak strain dwell-period of 60 s (0/60), (c) with tension/compression peak strain dwell-period of 30 s (30/30) and (d) the simulated result of stress evolution with time.

6. Results and discussions

6.1 Parametric sensitivity study

A parametric sensitivity study was performed to evaluate the capability of the kinematic hardening model for predicting the ratcheting and stress relaxation behavior. Here as a specific example of ratcheting deformation, the asymmetric strain-controlled fatigue loading was simulated with a stress amplitude of 990 MPa and stress ratio -0.8. A strain-controlled creep-fatigue loading was also simulated for analyzing the stress relaxation.

In Fig. 7, the sensitivity of the ratcheting response to changes in the parameters of η_0 and Z_2 are plotted. Figs. 7(a)-(c) show the calculated stress-strain curves when the parameter η_0 takes different values. It can be found that the larger the parameter η_0,

the more the accumulation of inelastic strain. The ratcheting strains at different loading cycles is shown in Fig. 7(d), confirming that the parameter η_0 markedly affects the growth rate of ratcheting strain, and there is a positive correlation between the η_0 and ratcheting strain. In contrast, for given number of cycles, the larger the parameter Z_2, the smaller the ratcheting strain, but the effect is not pronounced unless prolonged loading is encountered, as shown in Fig. 7(e)-(f).

In Fig. 8, the sensitivity of the stress and strain response to changes of the parameters in the static recovery term is plotted. Recalling Eq. 15, it indicates that the value of the static recovery term is jointly determined by the parameters r_0 and φ_s, which can be confirmed from Figs. 8(a)-(d). Increasing the values of r_0 and φ_s can produce more pronounced stress relaxation response. On the contrary, decreasing parameter ρ_r enhances the stress relaxation as shown in Figs. 8(e)-(f). Another interesting numerical observation is that the degree of stress relaxation gradually rises with increasing number of cycles, but the difference between the stress relaxation responses with different values of ρ_r hardly changes at different cycles, as shown in Fig. 8(g)-(h).

The back stress in the crystal plasticity framework plays an important role for the cyclic loading condition. The sensitivity study of phenomenological parameters in the modified back stress model is presented in Figs. 7-8. It should be noted that it is meaningless to analyze the effect of the single phenomenological parameter mentioned above on the cycle characteristics. On the contrary, it is reasonable to discuss the effects of dynamic and static recovery terms determined by all phenomenological parameters on the cyclic characteristics. From the mathematical point of view, it can be concluded that the increasing dynamic recovery terms drives a gradual increase in the accumulated ratcheting strain. In addition, the degree of stress relaxation becomes more obvious with the increased absolute value of the static recovery term. The parametric sensitivity study can not only prove the capability of the proposed model for predicting the ratcheting and stress relaxation responses, but also provide a guidance for the subsequent development and improvement of the model.

It should be emphasized that the cyclic hardening behavior of material is affected by

multiple factors, including the linear hardening term, the dynamic recovery term and the static recovery term. In this section, the capability of kinematic hardening rule for predicting the ratcheting and stress relaxation behaviors was mainly concerned. Therefore, only the roles of dynamic and static recovery term were considered respectively.

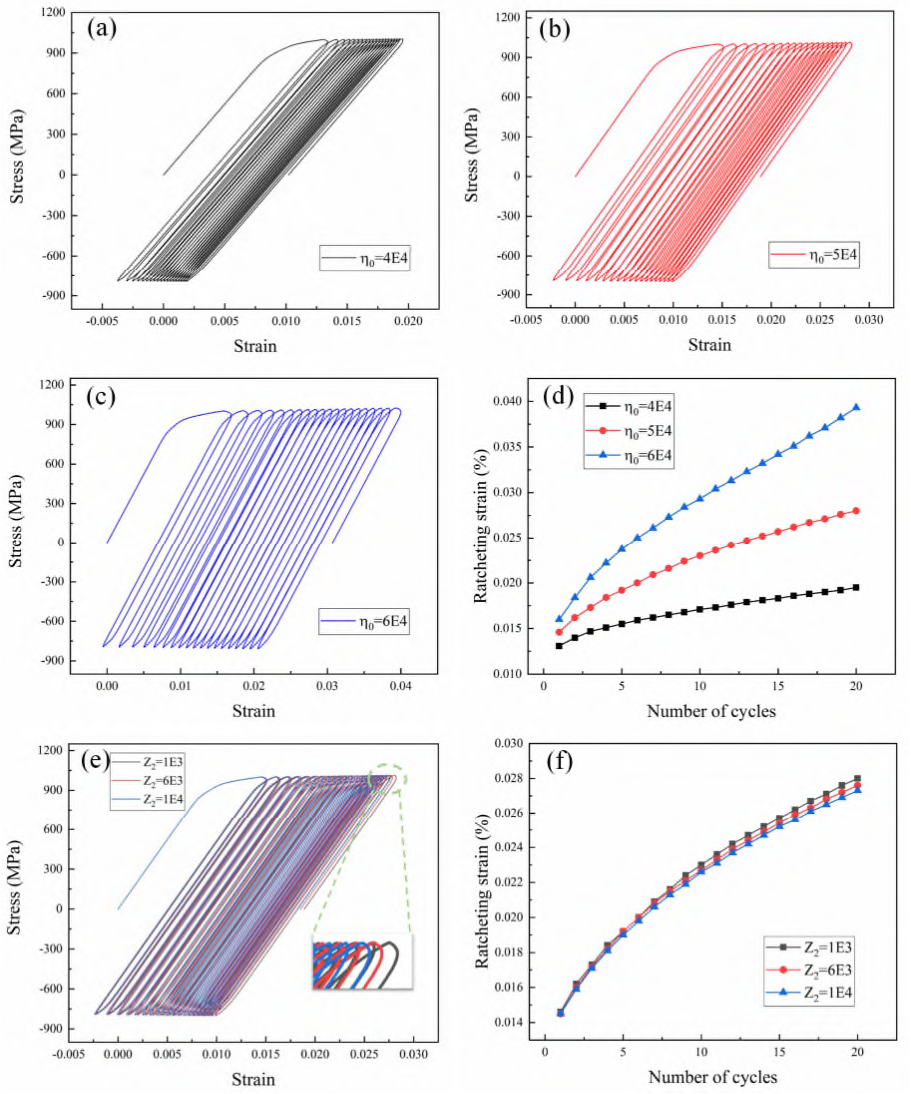

Fig. 7. The sensitivity analysis of the material parameters in the dynamic recovery term for the kinematic hardening rule. (a)-(d) The effects of parameters η_0 on the stress-strain curve and ratcheting strain. (e)-(f) The effects of parameters Z_2 on the stress-strain curve and ratcheting strain.

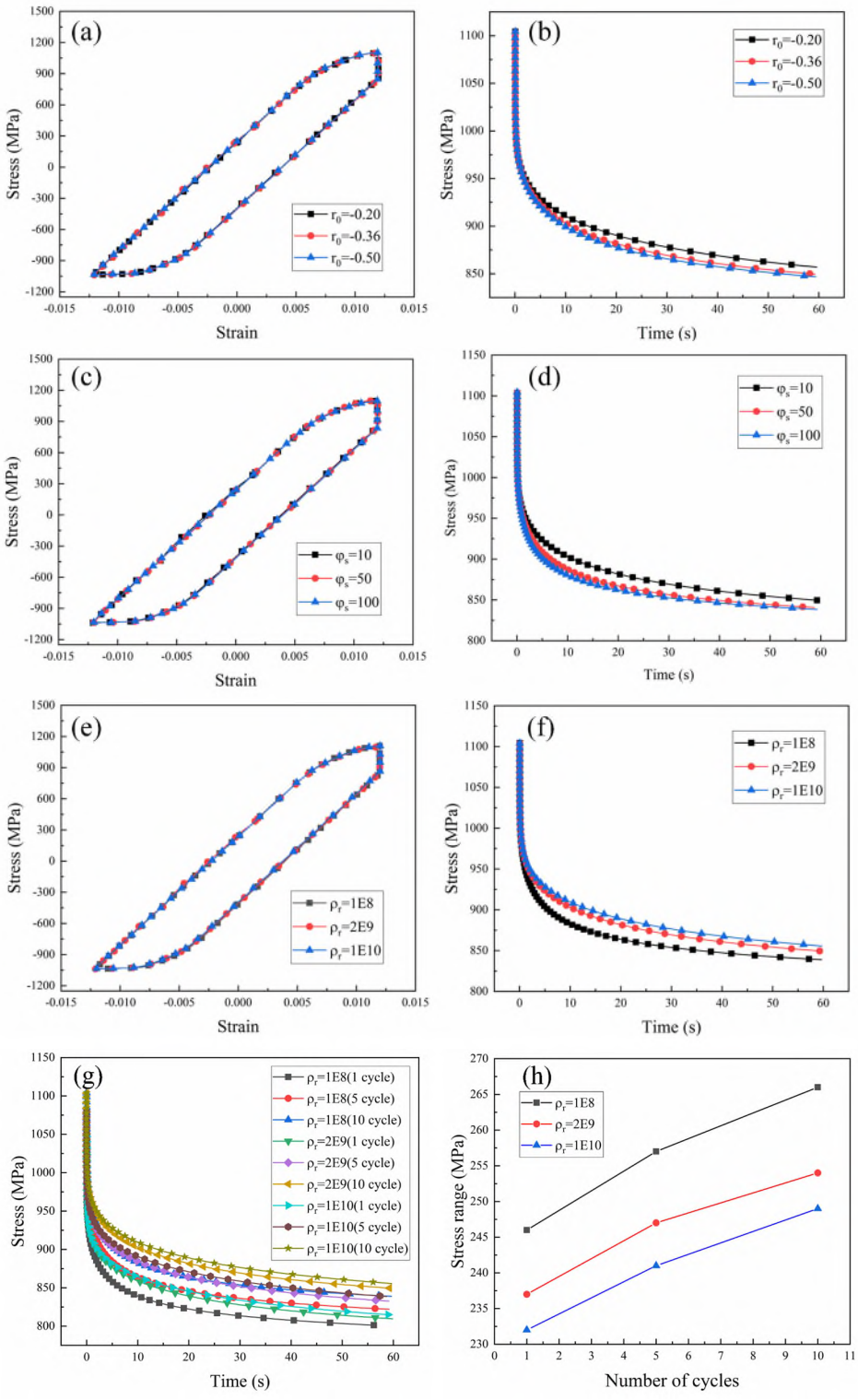

Fig. 8. The sensitivity analysis of the material parameters in the static recovery term of the kinematic hardening rule. (a)-(f) The effects of parameters r_0, φ_s and ρ_r on the stress relaxation curve for the 10th cycle of the simulation, respectively. (g)-(h) The effects of changing parameter ρ_r on the stress relaxation range under typical cycle times.

6.2 Quantitative analysis of micro parameter evolution

The calculated dislocation density curves under strain-controlled fatigue loading with different strain amplitudes are plotted in Fig. 9(a). It is evident that the dislocation density increases with the strain amplitude. This could be attributed to the fact that the occurrence of dislocation entanglement is positively correlated with the degree of plastic deformation. The calculated dislocation density remains constant when the loading direction is changed and the yield stress is not reached. It should be emphasized that the mechanism of dislocation density annihilation caused by reverse loading has not been considered in this work, which will be addressed in future work. The calculated dislocation density under creep-fatigue loading is shown in Figs. 9(b)-(d). The most obvious feature is that the dislocation density slowly increases during the strain dwell stage. In previous microscopic characterization of Ni-based alloys DZ445 [85], it was fewer dislocation features were observed at a short dwell-period. In addition, the microscopic characteristics of Ni-based alloys after long-term stress relaxation tests were analyzed [67], and the results showed that the accumulation and entanglement of dislocations will lead to a gradual increase in dislocation density. With the extension of strain dwell-period, the mobile dislocations density decreases gradually under the hindering effect of precipitates on dislocations, so that the stress relaxation state gradually tends to be stable, which is consistent with the results shown in Fig. 8.

It should be noted that accurate statistics of dislocation density are difficult, leading to the fact that the calculated dislocation density is not necessarily in complete agreement with the experimental results. Nevertheless, the proposed model can capture the evolution trend of dislocation density. Therefore, the above results can still provide some guidance for further understanding the microscopic mechanisms of single crystal materials under strain-controlled fatigue and creep-fatigue conditions.

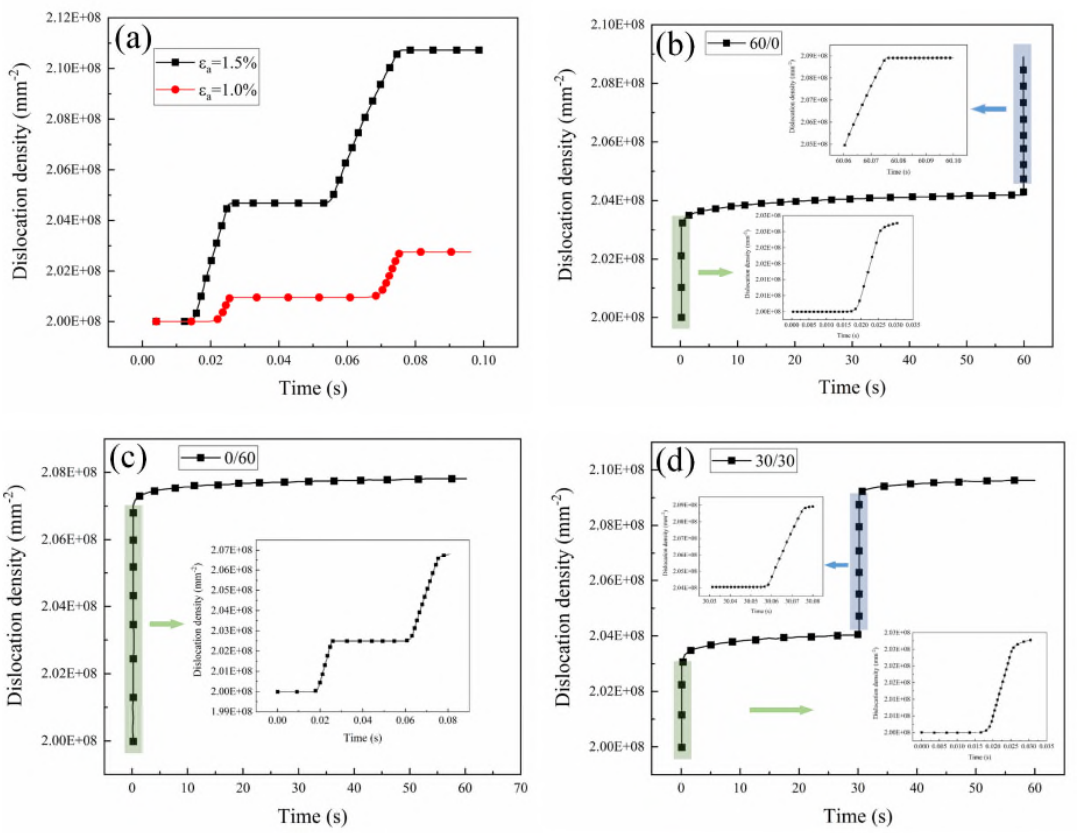

Fig. 9. The evolution of dislocation density parameters under different loading conditions: (a) without dwell-period (0/0), (b) with tension peak strain dwell-period of 60 s (60/0), (c) with compression peak strain dwell-period of 60 s (0/60) and (d) with tension/compression peak strain dwell-period of 30 s (30/30).

6.3 Existing life prediction methods

Limited by the analysis method, macro parameters such as stress-strain amplitude, and maximum stress value were regarded as input variables in the earlier life prediction models. Empirical formula theory and extensive experimental data were the basis for life prediction models, and the physical processes leading to failure were not considered in the models, such as the traditional Manson-Coffin equation. Shi et al. [79] conducted a study on the influence of dwell types on the fatigue life of Ni-based single crystal superalloy DD6. Additionally, they compared the predicted results of an energy-based life prediction model and a life prediction model based on the Manson-Coffin equation, as illustrated in Fig. 10. It can be observed that the predicted results falls within the scatter band of factor ± 6 and ± 11 compared to experimental results, indicating that these empirically derived life prediction models cannot accurately capture the creep-

fatigue life characteristics of DD6.

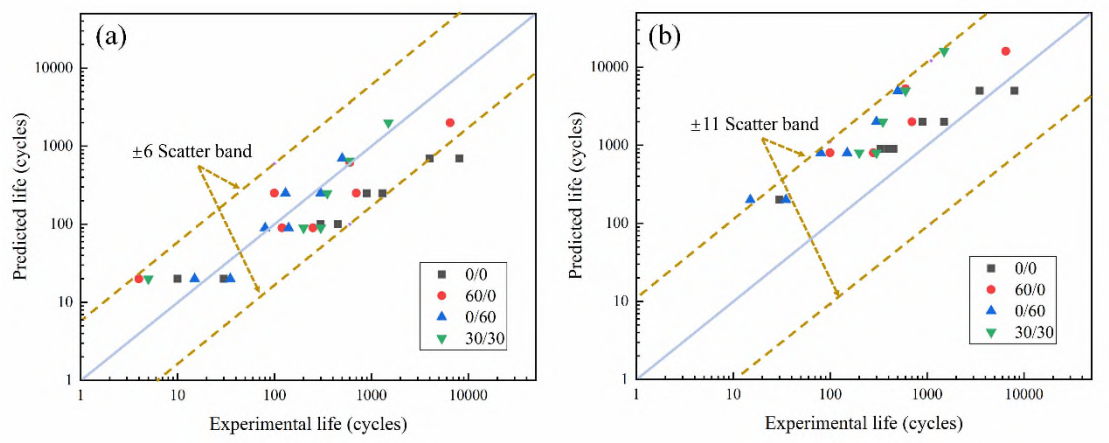

Fig. 10. Comparisons between experimental and predicted life of uniaxial creep-fatigue testing on DD6 superalloy at 760 °C: the existing life prediction methods based on (a) energy and (b) Manson-Coffin model. (Data sourced from Ref. [79])

The continuous development of microstructural characterization techniques has laid the foundation for establishing damage-based life prediction models. Several methods of building life prediction models are summarized in Fig. 11. The characterization of damage parameters and the description of damage evolution law have become the main theoretical basis and method for establishing life prediction models because of the more explicit physical significance. Generally speaking, there are two main methods to describe the damage degree of materials under cyclic loading conditions. The first method is to consider that the accumulated damage degree of each cycle in the whole loading cycle is equal and approximately equal to the corresponding damage value when the hysteretic loading curve reaches a steady state. This method can be called as half-life concept model. Another method is to accurately calculate the damage value generated in each cycle. When the accumulated damage value reaches a critical value, the corresponding number of cycles is considered to be the life of the material. This method can be called as cycle-by-cycle concept model. The former method only needs to obtain the steady-state hysteresis loop curve to predict the life, which sacrifices some prediction accuracy but is easier to implement. The latter method, which requires analysis of the loading curve over the entire lifetime, can theoretically improve the prediction accuracy of the model. However, more factors need to be considered, which

increases the computational complexity and is not easy to implement. With the development of finite element technology, the damage accumulation of materials can be calculated with the help of a computer, which eases the difficulty of using the cycle-by-cycle concept model to a certain extent. However, the computational resources and time required for CPFEM calculations on complex components are enormous. Therefore, it is unrealistic to predict the cyclic loading curve of the entire lifetime for long-time loading conditions through CPFEM such as fatigue loading. The most common approach was to obtain the steady-state hysteresis loop curve by the finite element method, which usually requires only a small number of cycles [16]. Therefore, the half-life concept was adopted in this study in order to build a life prediction model that was convenient for engineering application. Furthermore, the coupling rules of creep and fatigue damage were discussed in the next section.

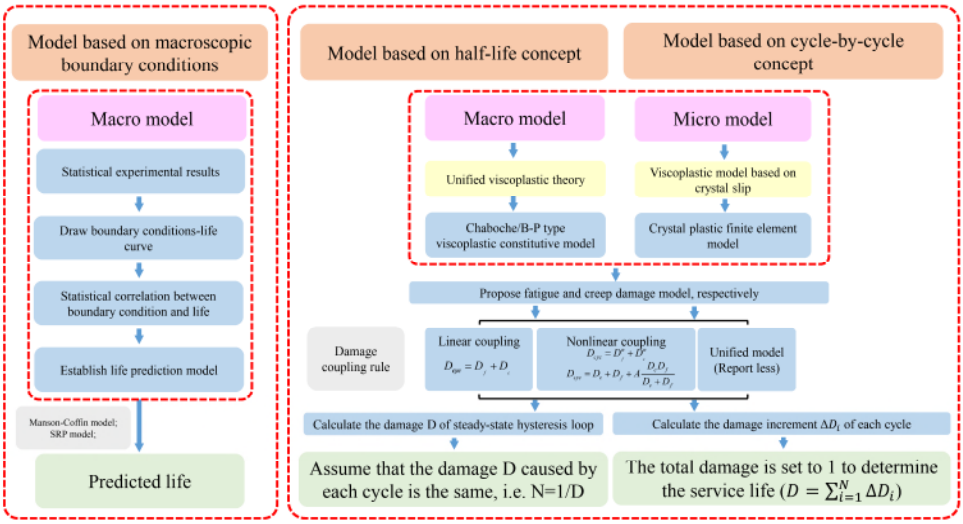

Fig. 11. Typical technical routes and contents of life prediction methods of alloys.

6.4 Proposed life prediction model based on LDS rule

Several common ideas for building life prediction models have been introduced in Section 6.3. There is no doubt that the application of the CPFEM is beneficial for understanding the failure mechanism of single crystal materials under fatigue loading and establishing a more accurate life prediction model. However, the computational efficiency of the CPFEM is lower than that of the unified viscoplastic constitutive model, which limits the application prospects of the crystal plasticity model. In the

crystal plasticity framework, it is impractical to use the cycle-by-cycle concept model because it requires the calculation of the entire fatigue cycle. Therefore, the half-life concept model that only needs to calculate the steady-state hysteresis loop curve was accepted for constructing the life prediction model. The schematic diagram of steady-state hysteresis loop for damage and life prediction is plotted in Fig. 12. The tenth hysteresis loop of the calculated results was considered as the steady-state hysteresis loop in this work. The steady-state hysteresis loop was divided into five parts, of which the second and fourth parts were used to calculate the creep damage, and the remaining three parts were used to calculate the fatigue damage. Fatigue damage and creep damage are calculated by Eqs. 22 and 25, respectively. So far, there is no unified explanation for the coupled damage mechanism under creep-fatigue loading. There is such a fact that the creep-fatigue life distribution of metallic materials is dispersive. Therefore, it is reasonable that the LDS rule is accepted to calculate damage and life prediction, that is, the damage of the material is defined as a linear accumulation of fatigue damage and creep damage. Based on the above discussion, the predicted creep-fatigue life can be written as

$$N_{c-p} = \frac{1}{D_c + D_f} \tag{25}$$

where D_c and D_f are creep damage and fatigue damage, respectively. N_{c-p} is creep-fatigue life.

Previous research proved that the damage of the steady-state hysteretic loop could not represent the initial stage at small strain amplitudes [86], and hence the prediction results of the half-life concept model are dependent on the strain amplitude. To capture this effect in our model, the parameter B_1 in Eq. 24 was considered to be related to the strain amplitude (ε_a) i.e., $B_1 = 389501 - 630849 \times \varepsilon_a + 257797 \times \varepsilon_a^2$. It should be emphasized that the creep-fatigue life data of tension peak strain dwell-period of 60 s with different strain amplitudes were used for model calibration. Other creep-fatigue loading conditions were employed as validation data to verify the accuracy of the model. The comparison between experimental and predicted life based on the established life

model is plotted in Fig. 13. Most of the data points lied within a scatter band of factor ±2, which demonstrates that compared to the empirically derived life prediction model shown in Fig. 10, the life prediction model proposed in this work can accurately predict the strain-controlled uniaxial fatigue and creep-fatigue life of Ni-based single crystals.

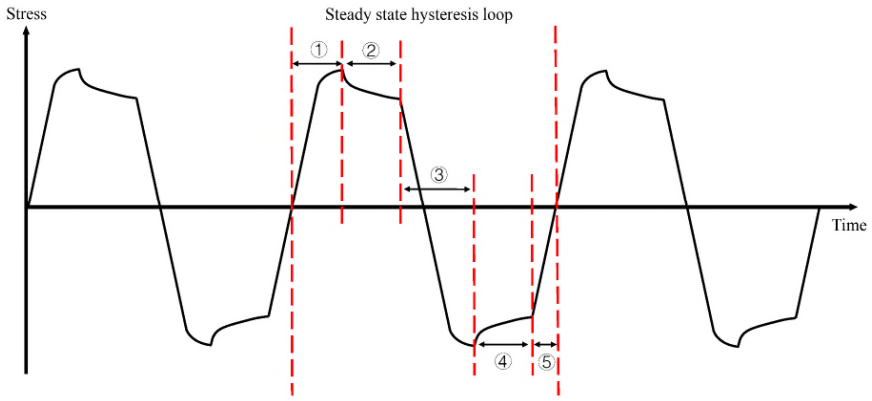

Fig. 12. Schematic diagram of steady-state hysteresis loop for damage and life prediction. Among them, part one, three and five are used to calculate fatigue damage. The part two and four are used to calculate creep damage.

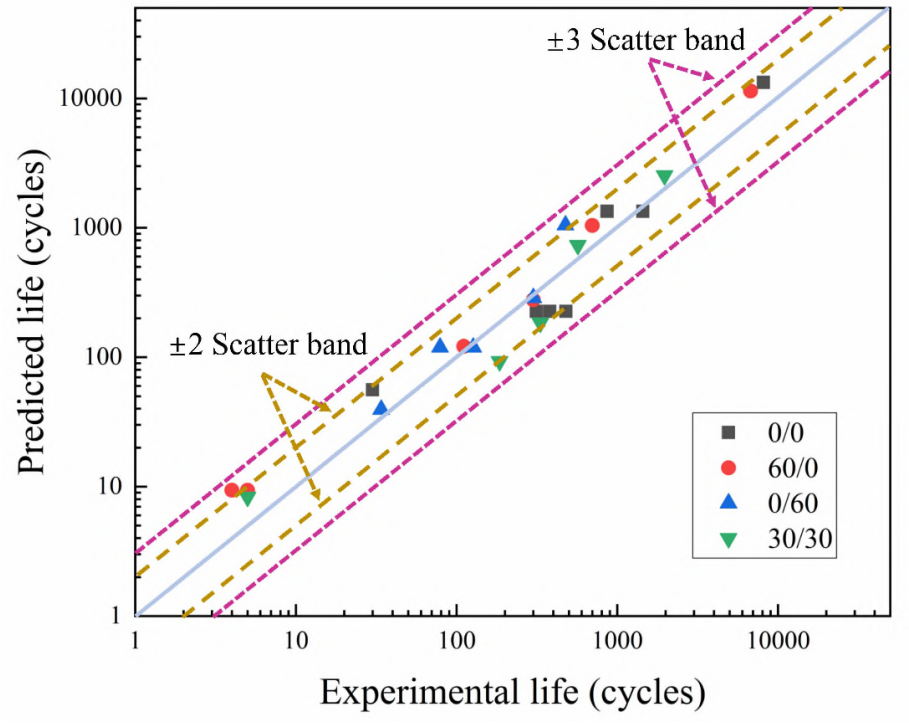

Fig. 13. Comparisons between experimental and predicted life.

6.5 Conservative life prediction model based on NDS rule

The LDS rule discussed in Section 6.4 is extended to more general NDS rule for different engineering applications. A common NDS rule is shown in Eq. 26 [12]. A

schematic diagram of the creep-fatigue interaction for different design rules is plotted in Fig. 14. The safety design region of NDS rules are obviously smaller than that of LDS rule, which represents a more conservative prediction result. Fig. 15 shows the comparison between the predicted life based on NDS rule and the experimental results. It can be concluded that the prediction life based on the NDS rules are more conservative than that of the LDS rules, which is beneficial to ensure the safe operation of the components. Furthermore, a higher power exponents result in more conservative calculation results in NDS rules. Safety is the most important factor in engineering applications. Although NDS rules cannot fully exploit the properties of materials, the better security makes the NDS rules more likely to be accepted in engineering applications. As a result, the application prospect of NDS rules, which can obtain safer prediction results, is wider than that of LDS rules. Therefore, it is more reasonable to choose NDS rules for some special materials and applications.

$$N_{c-f} = \frac{1}{D_c^{\,q} + D_f^{\,q}} \tag{26}$$

where q is the power exponent, which can be adjusted according to actual needs.

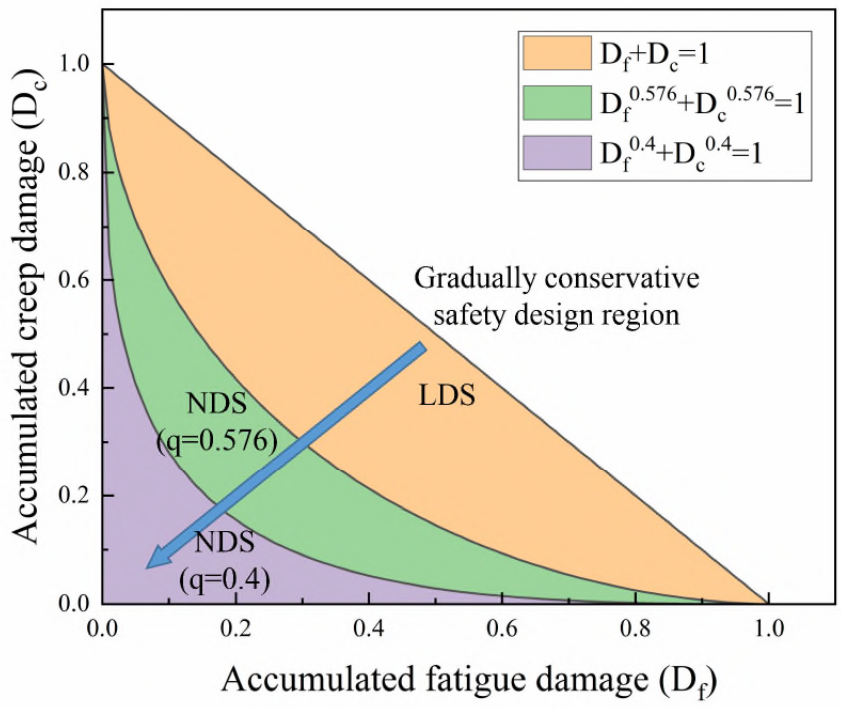

Fig. 14. Creep-fatigue interaction diagram using LDS and NDS rules.

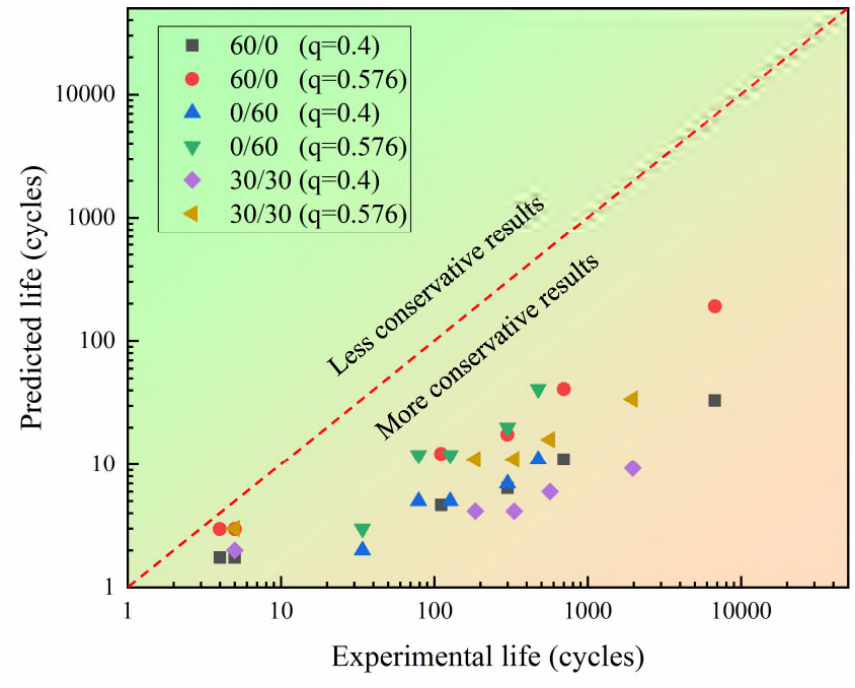

Fig. 15. Comparisons between experimental and predicted life following the NDS rule with different degrees of conservatism.

The LDS and NDS rules were used to assess the combined creep and fatigue damage, providing accurate and conservative methods for life prediction, respectively. The limitation is that the coupling physical mechanism of creep and fatigue process has not been considered in the current model, which requires establishment of fundamental understanding for the formulation of a coupled constitutive model, and hence future work could be devoted to revealing the creep-fatigue coupling mechanism.

7. Conclusions

Crystal plasticity constitutive model and thermodynamics informed creep-fatigue life model were developed to predict the response of Ni-based single crystal to cyclic loads. In this modelling framework, a new kinematic hardening rule considering dislocation density was proposed. The main conclusions are drawn as follows:

(1) The proposed crystal plasticity constitutive model can accurately capture the ratcheting and stress relaxation behaviors of Ni-based single crystals DD6 through the improved kinematic hardening rule. The parametric sensitivity study proves the excellent predictive capability of the model for ratcheting and stress relaxation behavior.

(2) Thermodynamics entropy generation can be used as an important index to

describe the performance degradation of materials. The fatigue and creep damage models based on thermodynamic entropy generation achieved high accuracy to evaluate the damage degree of Ni-based single crystal under creep-fatigue interaction.

(3) The linear and nonlinear damage summation rules were introduced into the creep-fatigue damage interaction diagram to compare different creep-fatigue interaction models and achieve more accurate or more conservative life predictions. Most of the predicted result falls within a scatter band of factor 2.0, which proves that the life prediction model based on the LDS rule has a good prediction accuracy for strain-controlled fatigue and creep-fatigue life. The life prediction approach based on NDS rule is suitable for obtaining more conservative prediction results.

Acknowledgements

This work is supported by National Science and Technology Major Project (J2019-IV-0003-0070), the National Natural Science Foundation of China (12102320) and China Postdoctoral Science Foundation (2021M692571).

Appendix A

In the author's previous work [52], a dislocation density-based single crystal plasticity constitutive model was proposed to describe the uniaxial behavior of Ni-based single crystals. A variety of strengthening mechanisms were considered in the model. The thermally activated cross-slip mechanism was used to capture the anomalous yield behavior. The transformation of dislocation motion mode was described via a temperature dependent function. This work mentioned in Appendix A provides a basis for accurately describing and predicting the cyclic loading behavior of Ni-based single crystals. The main equations of the single crystal constitutive model are summarized as follows.

The current strength of slip system α consists of g_0^α and g_{for}^α. The initial slip resistance g_0^α is related to the yield stress. The slip resistance g_{for}^α mainly controls the work hardening behavior of materials.

$$g^{\alpha} = g_0^{\alpha}(T) + g_{for}^{\alpha}(T) \tag{A1}$$

The initial slip resistance g_0^{α} is determined by a variety of deformation mechanisms, which can be expressed as follow.

$$g_0^{\alpha}(T) = g_{0,ss}^{\alpha}(T) + g_{0,shear}^{\alpha}(T) + g_{0,loop}^{\alpha}(T) \tag{A2}$$

The multi-component solid solution hardening model is as follows.

$$g_{0,ss}^{\alpha}(T) = \frac{1}{M}\sum \frac{d\sigma}{d\sqrt{g_i}}\sqrt{g_i} \tag{A3}$$

The contribution of the shearing mechanism to the initial slip resistance is as follows.

$$g_{0,shear}^{\alpha}(T) = \tau_{0,APB}^{\alpha}(T) + \tau_{0,cs}^{\alpha}(T) \tag{A4}$$

where

$$\tau_{0,APB}^{\alpha}(T) = 0.7G_{\gamma'}\left(\frac{APB_{\gamma'}^{\alpha}}{G_{\gamma'}^{\alpha}b_{\gamma'}^{\alpha}}\right)^{\frac{3}{2}}\left(\frac{af_{shear}r_{\gamma'}}{b_{\gamma'}^{\alpha}}\right)^{\frac{1}{2}} \tag{A5}$$

$$APB_{\gamma'}^{\alpha}(T) = APB_{\gamma'}^{\alpha}(T_0)\frac{f(T)}{f(T_0)}\left(\frac{1+\int_0^{T_0}\bar{\alpha}(T)dT}{1+\int_0^{T}\bar{\alpha}(T)dT}\right)^2\left(1-\frac{\int_{T_0}^{T}C_V(T)dT}{\int_{T_0}^{T_B}C_V(T)dT+\Delta H_M+\Delta H_B}\right) \tag{A6}$$

$$\tau_{0,cs}^{\alpha}(T) = f[\tau_{Ni_3Al}(T) + \frac{1}{M}\sum_i\left(\frac{d\sigma}{dC_i}C_i\right)] \tag{A7}$$

$$\tau_{Ni_3Al}(T) = B\exp[-\frac{(T-T_r)^2}{\xi}] \tag{A8}$$

The contribution of the by-passing mechanism to the initial slip resistance is as follows.

$$g_{0,loop}^{\alpha}(T) = \frac{1}{M}\frac{0.3Gb\sqrt{f_{loop}}}{r}\ln\left(\frac{r}{2b}\right) \tag{A9}$$

where

$$p(T) = \begin{cases} \dfrac{\sigma_{\gamma'}(T)-\sigma_{\gamma}(T)}{2(\sigma_{\gamma'}(T)+\sigma_{\gamma}(T))} & \sigma_{\gamma'}(T) > \sigma_{\gamma}(T) \\ 0 & \sigma_{\gamma'}(T) \le \sigma_{\gamma}(T) \end{cases} \tag{A10}$$

$$f_{loop}(T) = p(T)f(T) \tag{A11}$$

$$f_{shear}(T) = (1-p(T))f(T) \tag{A12}$$

The slip resistance g_{for}^{α} is given by

$$g_{for}^{\alpha}(T)=b^{\alpha}G^{\alpha}(T)\sqrt{h^{\alpha\alpha'}\rho_{for}^{\alpha'}} \tag{A13}$$

Appendix B

The cross-slip induced hardening constants and strengthening coefficient are required in the calculation of single crystal constitutive model, which are summarized in Tables B1 and B2 respectively for easy reference. More detailed information can be found in the author's previous work [52].

Table B1. The cross-slip induced hardening constants $d\sigma/dC_i$ of some alloying elements.

Elements	Al	Cr	Co	Mo	Ti	V	W	Hf	Ta
Coefficient (MPa/pct)	0	7	0	16.8	25	8.2	12.1	62.2	11.3

Table B2. The strengthening coefficient $d\sigma/d\sqrt{g_i}$ of typical elements.

Elements	Cr	Co	Mo	W	Ta	Al
Coefficient($\mathrm{MPa}/\sqrt{\mathrm{frac}}$)	337	39.4	1015	977	1191	225

References

[1] Z. Liu, J.-G. Gong, P. Zhao, X.-C. Zhang, F.-Z. Xuan, Creep-fatigue interaction and damage behavior in 9-12%Cr steel under stress-controlled cycling at elevated temperature: Effects of holding time and loading rate, International Journal of Fatigue 2022;156:106684.

[2] J. Kumar, A. Venugopal Rao, S. Ganesh Sundara Raman, V. Kumar, Creep-fatigue damage simulation at multiple length scales for an aeroengine titanium alloy, International Journal of Fatigue 2018;116:505-512.

[3] K. Song, K. Wang, L. Zhang, L. Zhao, L. Xu, Y. Han, K. Hao, Insights on low cycle fatigue crack formation and propagation mechanism: A microstructurally-sensitive modeling, International Journal of Plasticity 2022;154:103295.

[4] Z. Wang, W. Wu, J. Liang, X. Li, Creep–fatigue interaction behavior of nickel-based single crystal superalloy at high temperature by in-situ SEM observation, International Journal of Fatigue 2020;141:105879.

[5] L.F. Coffin, Predictive parameters and their application to high temperature, low cycle fatigue, Fracture London Chapman & Hall 2013;1:1-10.

[6] C.L. F, Concept of frequency separation in life prediction for time-dependent fatigue Master 1976;4093:1-10.

[7] O. W.J., A Damage Function and Associated Failure Equations for Predicting Hold Time and Frequency Effects in Elevated Temperature, Low Cycle Fatigue, Journal of Testing and Evaluation 1976;4:327-339.

[8] B. Ding, W. Ren, Y. Zhong, X. Yuan, T. Zheng, Z. Shen, Y. Guo, Q. Li, J. Peng, J. Brnic, Y. Gao, P.K. Liaw, Revealing the influential mechanism of strain ranges on cyclic-life saturation during creep-fatigue in Nickel-based superalloy DZ445, International Journal of Plasticity 2022;155:103320.

[9] K.-S. Li, R.-Z. Wang, X.-C. Zhang, S.-T. Tu, Creep-fatigue damage mechanisms and life prediction based on crystal plasticity combined with grain boundary cavity model in a nickel-based superalloy at 650°C, International Journal of Plasticity 2023;165:103601.

[10] R. E.L., Effect of temperature variation on the long-time rupture strength of steels, Trans ASME 1952;74:777-781.

[11] R.-Z. Wang, X.-C. Zhang, S.-T. Tu, S.-P. Zhu, C.-C. Zhang, A modified strain energy density exhaustion model for creep–fatigue life prediction, International Journal of Fatigue 2016;90:12-22.

[12] K.-S. Li, R.-Z. Wang, G.-J. Yuan, S.-P. Zhu, X.-C. Zhang, S.-T. Tu, H. Miura, A crystal plasticity-based approach for creep-fatigue life prediction and damage evaluation in a nickel-based superalloy, International Journal of Fatigue 2021;143:106031.

[13] R.-Z. Wang, S.-J. Guo, H. Chen, J.-F. Wen, X.-C. Zhang, S.-T. Tu, Multi-axial creep-fatigue life prediction considering history-dependent damage evolution: A new numerical procedure and experimental validation, Journal of the Mechanics and Physics of Solids 2019;131:313-336.

[14] L. Xu, R.-Z. Wang, J. Wang, L. He, T. Itoh, H. Miura, X.-C. Zhang, S.-T. Tu, On multiaxial creep–fatigue considering the non-proportional loading effect: Constitutive

modeling, deformation mechanism, and life prediction, International Journal of Plasticity 2022;155:103337.

[15] L. Xu, L. Zhao, Z. Gao, Y. Han, A novel creep–fatigue interaction damage model with the stress effect to simulate the creep-fatigue crack growth behavior, International Journal of Mechanical Sciences 2017;130:143-153.

[16] A. Staroselsky, B.N. Cassenti, Creep, plasticity, and fatigue of single crystal superalloy, International Journal of Solids and Structures 2011;48:2060-2075.

[17] L. Taleb, G. Cailletaud, Cyclic accumulation of the inelastic strain in the 304L SS under stress control at room temperature: Ratcheting or creep?, International Journal of Plasticity 2011;27:1936-1958.

[18] J. Svoboda, F.D. Fischer, H. Riedel, E. Kozeschnik, Precipitate growth in multi-component systems with stress relaxation by diffusion and creep, International Journal of Plasticity 2016;82:112-126.

[19] M. Xie, G. Chen, A developed crystal plasticity model for viscoplastic mechanical behavior of SAC305 solder under thermomechanical coupled cyclic loading, International Journal of Plasticity 2022;159:103465.

[20] E.A. Estrada Rodas, R.W. Neu, Crystal viscoplasticity model for the creep-fatigue interactions in single-crystal Ni-base superalloy CMSX-8, International Journal of Plasticity 2018;100:14-33.

[21] S.-L. Zhang, F.-Z. Xuan, Interaction of cyclic softening and stress relaxation of 9-12% Cr steel under strain-controlled fatigue-creep condition: Experimental and modeling, International Journal of Plasticity 2017;98:45-64.

[22] W. Cao, J. Yang, H. Zhang, Unified constitutive modeling of Haynes 230 including cyclic hardening/softening and dynamic strain aging under isothermal low-cycle fatigue and fatigue-creep loads, International Journal of Plasticity 2021;138:102922.

[23] E. Contesti, G. Cailletaud, Description of creep-plasticity interaction with non-unified constitutive equations: application to an austenitic stainless steel, Nuclear Engineering and Design 1988;116:265-280.

[24] D.-L. Wu, F.-Z. Xuan, S.-J. Guo, P. Zhao, Uniaxial mean stress relaxation of 9-12% Cr steel at high temperature: Experiments and viscoplastic constitutive modeling,

International Journal of Plasticity 2016;77:156-173.

[25] J.L. Chaboche, On some modifications of kinematic hardening to improve the description of ratchetting effects, International Journal of Plasticity, 1991;7:661-678.

[26] J.L. Chaboche, A review of some plasticity and viscoplasticity constitutive theories, International Journal of Plasticity 2008;24:1642-1693.

[27] N. Ohno, J.-D. Wang, Kinematic hardening rules with critical state of dynamic recovery, Parts I, International Journal of Plasticity 1993;9:375-390.

[28] D.L. McDOWELL, Stress state dependence of cyclic ratchetting behavior of two rail steels, International Journal of Plasticity 1995;11:397-421.

[29] N. Ohno, M. Abdel-Karim, Uniaxial ratchetting of 316FR steel at room temperature- Part II: constitutive modeling and simulation, J. Engng. Mater. Technol. 2000;122:35-41.

[30] H. Li, C. Yu, G. Kang, Crystal plasticity modeling of the multiaxial ratchetting of extruded AZ31 Mg alloy, International Journal of Plasticity 2022;152:103242.

[31] Y. Dong, G. Kang, C. Yu, A dislocation-based cyclic polycrystalline visco-plastic constitutive model for ratchetting of metals with face-centered cubic crystal structure, Computational Materials Science 2014;91:75-82.

[32] B. Zhang, R. Wang, D. Hu, K. Jiang, X. Hao, J. Mao, F. Jing, Constitutive modelling of ratcheting behaviour for nickel-based single crystal superalloy under thermomechanical fatigue loading considering microstructure evolution, International Journal of Fatigue 2020;139:105786.

[33] D. Leidermark, M. Segersäll, Modelling of thermomechanical fatigue stress relaxation in a single-crystal nickel-base superalloy, Computational Materials Science 2014;90:61-70.

[34] C. Stöcker, M. Zimmermann, H.J. Christ, Z.L. Zhan, C. Cornet, L.G. Zhao, M.C. Hardy, J. Tong, Microstructural characterisation and constitutive behaviour of alloy RR1000 under fatigue and creep–fatigue loading conditions, Materials Science and Engineering: A 2009;518:27-34.

[35] R. Hill, J.R. Rice, Constitutive analysis of elastic-plastic crystals at arbitrary strain, Journal of the Mechanics and Physics of Solids 1972;20:401-413.

[36] H. Farooq, G. Cailletaud, S. Forest, D. Ryckelynck, Crystal plasticity modeling of the cyclic behavior of polycrystalline aggregates under non-symmetric uniaxial loading: Global and local analyses, International Journal of Plasticity 2020;126:102619.

[37] J. Gao, H. Li, X. Sun, X. Zhang, M. Zhan, Electro-thermal-mechanical coupled crystal plasticity modeling of Ni-based superalloy during electrically assisted deformation, International Journal of Plasticity 2022;157:103397.

[38] A.S. Khan, J. Liu, A deformation mechanism based crystal plasticity model of ultrafine-grained/nanocrystalline FCC polycrystals, International Journal of Plasticity 2016;86:56-69.

[39] C.M.A. Iftikhar, Y.L. Li, C.P. Kohar, K. Inal, A.S. Khan, Evolution of subsequent yield surfaces with plastic deformation along proportional and non-proportional loading paths on annealed AA6061 alloy: Experiments and crystal plasticity finite element modeling, International Journal of Plasticity 2021;143:102956.

[40] B.L. Hansen, I.J. Beyerlein, C.A. Bronkhorst, E.K. Cerreta, D. Dennis-Koller, A dislocation-based multi-rate single crystal plasticity model, International Journal of Plasticity 2013;44:129-146.

[41] Y.Z. Li, M.X. Huang, A dislocation-based flow rule with succinct power-law form suitable for crystal plasticity finite element simulations, International Journal of Plasticity 2021;138:102921.

[42] J. Preußner, Y. Rudnik, H. Brehm, R. Völkl, U. Glatzel, A dislocation density based material model to simulate the anisotropic creep behavior of single-phase and two-phase single crystals, International Journal of Plasticity 2009;25:973-994.

[43] Y. Guan, B. Chen, J. Zou, T.B. Britton, J. Jiang, F.P.E. Dunne, Crystal plasticity modelling and HR-DIC measurement of slip activation and strain localization in single and oligo-crystal Ni alloys under fatigue, International Journal of Plasticity 2017;88:70-88.

[44] Z.L. Liu, Z. Zhuang, X.M. Liu, X.C. Zhao, Z.H. Zhang, A dislocation dynamics based higher-order crystal plasticity model and applications on confined thin-film plasticity, International Journal of Plasticity 2011;27:201-216.

[45] F. Yin, S. Hu, R. Xu, X. Han, D. Qian, W. Wei, L. Hua, K. Zhao, Strain rate

sensitivity of the ultrastrong gradient nanocrystalline 316L stainless steel and its rate-dependent modeling at nanoscale, International Journal of Plasticity 2020;129:102696.
[46] C.A. Sweeney, B. O'Brien, F.P.E. Dunne, P.E. McHugh, S.B. Leen, Strain-gradient modelling of grain size effects on fatigue of CoCr alloy, Acta Materialia 2014;78:341-353.
[47] X. Lu, F.P.E. Dunne, Y. Xu, A crystal plasticity investigation of slip system interaction, GND density and stored energy in non-proportional fatigue in Nickel-based superalloy, International Journal of Fatigue 2020;139:105782.
[48] B. Chen, J. Jiang, F.P.E. Dunne, Is stored energy density the primary meso-scale mechanistic driver for fatigue crack nucleation?, International Journal of Plasticity 2018;101:213-229.
[49] G.-J. Yuan, X.-C. Zhang, B. Chen, S.-T. Tu, C.-C. Zhang, Low-cycle fatigue life prediction of a polycrystalline nickel-base superalloy using crystal plasticity modelling approach, Journal of Materials Science & Technology 2020;38:28-38.
[50] D. Peirce, R.J. Asaro, A. Needleman, An analysis of nonuniform and localized deformation in ductile single crystals, Acta Metallurgica 1982;30:1087-1119.
[51] L.A. GYPEN, A. DERUYTTERE, Multi-component solid solution hardening, Journal of Materials Science 1977;12:1028-1033.
[52] P. Lu, Y.X. Ge, X.C. Jin, P. Li, X.K. Ji, D. Zhao, Z.H. Wang, X.L. Fan, A dislocation density-based model for the temperature dependent anomalous behaviors of nickel-based single-crystal superalloy, Mechanics of Materials 2022;170:104326.
[53] J. IRVINE, T.N. BAKER, The Influence of Rolling Variables on the Strengthening Mechanisms Operating in Niobium Steels, Materials Science and Engineering 1984;64:123-134.
[54] W. Li, J. Ma, H. Kou, J. Shao, X. Zhang, Y. Deng, Y. Tao, D. Fang, Modeling the effect of temperature on the yield strength of precipitation strengthening Ni-base superalloys, International Journal of Plasticity 2019;116:143-158.
[55] M.G. Lee, H. Lim, B.L. Adams, J.P. Hirth, R.H. Wagoner, A dislocation density-based single crystal constitutive equation, International Journal of Plasticity 2010;26:925-938.

[56] A. Arsenlis, D.M. Parks, Modeling the evolution of crystallographic dislocation density in crystal plasticity, Journal of the Mechanics and Physics of Solids 2002;50:1979-2009.

[57] U.F. Kocks, Laws for work-hardening and low-temperature creep, Journal of Engineering Materials and Technology 1976;98:76-85.

[58] U. Essmann, H. Mughrabi, Annihilation of dislocations during tensile and cyclic deformation and limits of dislocation densities, Philosophical Magazine A 2006;40:731-756.

[59] I.J. Beyerlein, C.N. Tomé, A dislocation-based constitutive law for pure Zr including temperature effects, International Journal of Plasticity 2008;24:867-895.

[60] M. Zecevic, M. Knezevic, A dislocation density based elasto-plastic self-consistent model for the prediction of cyclic deformation: Application to AA6022-T4, International Journal of Plasticity 2015;72:200-217.

[61] W. Prager, Recent developments in the mathematical theory of plasticity, Journal of Applied Physics 1949;20:235-241.

[62] C.O. Frederick, P.J. Armstrong, A mathematical representation of the multiaxial Bauschinger effect, Materials at High Temperatures 2007;24:1-26.

[63] J.L. CHABOCHE, Time-independent constitutive theories for cyclic plasticity, Imernattonal Journal of Plasticity 1986;2:149-188.

[64] G. Kang, Y. Dong, H. Wang, Y. Liu, X. Cheng, Dislocation evolution in 316L stainless steel subjected to uniaxial ratchetting deformation, Materials Science and Engineering: A 2010;527:5952-5961.

[65] M. Shenoy, Y. Tjiptowidjojo, D. McDowell, Microstructure-sensitive modeling of polycrystalline IN 100, International Journal of Plasticity 2008;24:1694-1730.

[66] M. Yaguchi, M. Yamamoto, T. Ogata, A viscoplastic constitutive model for nickel-base superalloy, part 1: kinematic hardening rule of anisotropic dynamic recovery, International Journal of Plasticity 2002;18:1083-1109.

[67] H. Jiang, J.X. Dong, M.C. Zhang, Z.H. Yao, J. Yang, Stress relaxation mechanism for typical nickel-based superalloys under service condition, Acta Metallurgica Sinica 2019;55:1212-1220.

[68] L. KACHANOV, Rupture time under creep conditions, International Journal of Fracture 1999;97:1-10.

[69] I.y. YF, Thermodynamic state of deformed solids. Report 1. Determination of local functions of state, Strength Mater 1984;16:238-241.

[70] M. Naderi, M.M. Khonsari, An experimental approach to low-cycle fatigue damage based on thermodynamic entropy, International Journal of Solids and Structures 2010;47:875-880.

[71] M. Amiri, M. Modarres, An Entropy-Based Damage Characterization, Entropy 2014;16:6434-6463.

[72] R. Idris, S. Abdullah, P. Thamburaja, M.Z. Omar, The need to generate entropy characteristics for fatigue life prediction in low-carbon steel, Journal of the Brazilian Society of Mechanical Sciences and Engineering 2018;40:408-418.

[73] H. Salimi, M. Pourgol-Mohammad, M. Yazdani, Metal fatigue assessment based on temperature evolution and thermodynamic entropy generation, International Journal of Fatigue 2019;127:403-416.

[74] Y. Duyi, W. Zhenlin, A new approach to low-cycle fatigue damage based on exhaustion of static toughness and dissipation of cyclic plastic strain energy during fatigue, International Journal of Fatigue 2001;23:679-687.

[75] W.M. Payten, D.W. Dean, K.U. Snowden, A strain energy density method for the prediction of creep–fatigue damage in high temperature components, Materials Science and Engineering: A 2010;527:1920-1925.

[76] Y.G. Huang, A User-Material Subroutine Incorporating Single Crystal Plasticity in the ABAQUS Finite Element Program. Mech Report 178, Division of Applied Sciences, Harvard University, Cambridge, MA., 1991.

[77] A.S. Khan, J. Liu, J.W. Yoon, R. Nambori, Strain rate effect of high purity aluminum single crystals: Experiments and simulations, International Journal of Plasticity 2015;67:39-52.

[78] L. Jiarong, L. Shizhong, W. Kaiguo, L. Cheng, Z. Zhengang, Tensile behavior of second generations single crystal superalloy DD6, Journal Iron and Steel Research 2003;15:272-275.

[79] D. Shi, J. Huang, X. Yang, H. Yu, Effects of crystallographic orientations and dwell types on low cycle fatigue and life modeling of a SC superalloy, International Journal of Fatigue 2013;49:31-39.

[80] X. Xiong, P. Dai, D. Quan, Z. Wang, Q. Zhang, Z. Yue, Intermediate temperature brittleness and directional coarsening behavior of nickel-based single-crystal superalloy DD6, Materials & Design 2015;86:482-486.

[81] H. Pei, Z. Wen, Z. Wang, W. Gan, G.X. Lu, Z. Yue, Transient thermal fatigue crack propagation behavior of a nickel-based single-crystal superalloy, International Journal of Fatigue 2020;131:105303.

[82] X. Xiong, D. Quan, P. Dai, Z. Wang, Q. Zhang, Z. Yue, Tensile behavior of nickel-base single-crystal superalloy DD6, Materials Science and Engineering: A 2015;636:608-612.

[83] C.a.m.m.e. committee, China aeronautical materials handbook, China aviation materials manual editorial committee, China Standards Press, 2002.

[84] F.L. Jing, Research on thermo-mechanical fatigue life assessment of single crystal turbine blades, Beijing: Beihang University; 2013.

[85] B. Ding, W. Ren, J. Peng, Y. Zhong, J. Yu, Influence of dwell time on the creep-fatigue behavior of a directionally solidified Ni-based superalloy DZ445 at 850 °C, Materials Science and Engineering: A 2018;725:319-328.

[86] R.Z. Wang, A creep-fatigue life prediction model based on strain energy density exhaustion criterion and its application on aero-engine turbine discs, Shanghai: East China University of Science and Technology; 2019.

Cranfield University

CERES Research Repository **https://dspace.lib.cranfield.ac.uk/**

School of Aerospace, Transport and Manufacturing (SATM) Staff publications (SATM)

Crystal plasticity constitutive model and thermodynamics informed creep-fatigue life prediction model for Ni-based single crystal superalloy

Lu, Pin

2023-07-23

Attribution-NonCommercial-NoDerivatives 4.0 International

Lu P, Jin X, Li P, et al., (2023) Crystal plasticity constitutive model and thermodynamics informed creep-fatigue life prediction model for Ni-based single crystal superalloy. International Journal of Fatigue, Volume 176, November 2023, Article number 107829

https://doi.org/10.1016/j.ijfatigue.2023.107829

Downloaded from CERES Research Repository, Cranfield University